リチウム二次電池用新規複合負極の開発

平 成 20 年 3 月

研究代表者　武 田 保 雄

（三重大学大学院工学研究科教授）

はじめに

インターカレーション材料はイオンの移動や貯蔵が起こる反応場が主に原子オーダーである。ゲストイオンを取り込むことのできる原子サイトの数は結晶構造で規定されるので、電極としての理論容量も同じ系統の構造をもつ材料であればほぼ同じ値に限られる。現行のリチウムイオン電池に使われている電極材料は優れているが、さらに大きなエネルギー密度と、ハイレート特性を持った電極材料の使用が望まれている。そこで、本研究ではインターカレーション電極としての従来の容量を超える様々な候補材料に注目し、その利点を 100%引き出そうとした。具体的にはリチウム電池用負極として注目されているリチウム窒化物（$Li_{2.6}Co_{0.4}N$ 等）、合金系負極（Si 等）、炭素系負極（熱分解炭素や MCMB 等）、酸化物負極（CoO 等）に注目した。これらは高容量負極として知られていたが、不可逆容量が大きい、サイクル特性が低いなどの実用上の欠点を有しており、実用電極材料として検討されるに至っていなかった。ここではそれぞれの利点を生かし、欠点を補うために、相互にナノオーダーで制御しながら複合化することでその欠点の解消を図った。さらにその電極反応の機構を検討し、黒鉛負極を大きく超える新しい高容量、高出力負極の開発を行った。

１．炭素材料マトリックス中へのナノサイズ合金系負極の均一分散によるサイクル性向上

容量の大きい合金系負極Siに注目し、それを炭素マトリックスに分散させることで、サイクル性の向上、初期不可逆容量の低減を目指した。Siを炭素マトリックス中に分散させる方法として、炭素前駆体とSi粉末とを混合して熱分解（900℃程度）と、高速ボールミル（HEMM）粉砕を組み合わせると、熱分解炭素マトリックスにSi-C複合負極が分散した組織が得られた。Poly Vinyl Chloride (PVC)を炭素前駆体とすることで性能向上が図られた

２．窒化物負極と合金系負極とのナノオーダーでの複合化による初期効率の改善とサイクル性の向上

Siは大きな容量が魅力であるが、粉末の状態ではサイクル特性と大きな初期不可逆容量が難点であった。我々は、以前、合金系負極Snやその酸化物SnOと窒化物を複合化することで初期不可逆容量を解消することが出来ることを見出している。そこで、Si粉末と窒化物、さらにグラファイト等第3成分を加えメカニカルミリングを加味してナノオーダーで複合化することで、サイクル性の向上をさらに図った。

3.新規負極の PEO 電解質系への適用

安全性の観点から、リチウム二次電池の電解質を有機電解液系から固体ポリマー電解質へ乗り換える動きが、最近盛んである。私たちのグループは長年、この研究テーマに取り組んできた。PEO系電解質は確かに安全性では優れているが、リチウムイオン導電率が低いという欠点とともに、有機電解液では有効であった黒鉛負極があまり有効に働かない点が大きな欠点であった。今回の研究で、上記、1.および 2 で開発された負極の PEO 電解質への適応を試み、有効な結果を得た。

研究組織

研究代表者　武田保雄　（三重大学大学院工学研究科教授）

研究分担者　今西誠之　（三重大学大学院工学研究科准教授）

研究分担者　平野 敦　（三重大学大学院工学研究科助教）

研究協力者　劉 宇　（三重大学大学院工学研究科雇用研究員）

研究協力者　花井一真　（三重大学大学院工学研究科博士後期課程学生）

交付決定額

	直接経費	間接経費	合計
平成 18 年度	7,100,000 円	2,130,000 円	9,230,000 円
平成 19 年度	7,000,000 円	2,100,000 円	9,100,000 円
総計	14,100,000 円	4,230,000 円	18,330,000 円

研究発表

（1） 雑誌論文

1. K.Hanai,Y.Liu,T.matsumura,N.Imanishi,A.Hirano,Y.Takeda, "Electrochemical behavior of the composite anodes consisting of carbonaceous materials and lithium transition-metal nitrides for lithium-ion batteries" Solid State Ionics, 2008 in press

2. N. Imanishi, Y. Ono, K. Hanai, R. Uchiyama, Y. Liu, A. Hirano, Y. Takeda, O. Yamamoto, "Surface-modified meso-carbon microbeads anode for dry polymer lithium-ion batteries" Journal of Power Sources, 178, 744-750 (2008)

3. J. Xie, N. Imanishi, A. Hirano, M. Matsumura, Y. Takeda, O. Yamamoto,"Orientation dependence of Li-ion diffusion kinetics in $LiCoO_2$ thin films prepared by RF magnetron sputtering" Solid State Ionics, 179, 362-370(2008)

4. J. Xie, N. Imanishi, A. Hirano, M. Matsumura, Y. Takeda, O. Yamamoto, "Kinetics investigation of a preferential (104) plane oriented $LiCoO_2$ thin film prepared by RF magnetron sputtering" Solid State Ionics, 178, 1218-1224(2007)

5.T.Matsumura,K.Nakano,R.Kanno,A.Hirano,N.Imanishi,Y.takeda, "Nickel sulfides as a cathode for all-solid-state ceramic lithium batteries" J. Power Sources, 174, 632-636(2007)

6. Y.Liu, Y.Takeda, T.Matsumura, J.Yang, N.Imanishi, O.Yamamoto, "Novel composite anodes consisting of lithium transition-metal nitrides and transition metal oxides for rechargeable Li-ion batteries." J.Electrochem.Soc., 153, A437-A444 (2006)

7. N.Imanishi, K.Shizuka, T.Ikenishi, T.Matsumura, A.Hirano, Y.Takeda, "Preparation and electorochemical properties of a Li_2CuO_2-Li_2NiO_2 solid solution as a lithium intercalation electrode" Solid State Ionics, 177, 1341-1346(2006)

(2)口頭発表

1. K. Hanai,Y. Liu, T. Matsumura, A. Hirano, N. Imanishi and Y. Takeda, "Influence of carbonaceous precursor upon morphological stability of Si/C composites for Li intercalation and extraction" 16th International Conference on Solid State Ionics, 2007.7.1-7　Shanghai

2. N. Imanishi, T. Saji, A. Hirano, Y. Takeda, O.Yamamoto, "Electrode-electrolyte interface design for low temperature all-solid polymer lithium cells" International Conference on "Polymer Batteries-Fuel Cells, PBFC-2007", 2007.6.4-6, Rome

3. 小野、劉、平野、今西、武田、PEO 全固体リチウム二次電池における黒鉛負極表面改質による特性改善、第 47 回　電池討論会、2006.11.20-22　東京

4. 武田、新しい二次電池電極、第 32 回固体イオニクス討論会、2006.11.28-29 福岡

研究成果

種々の投稿論文(英文)を編集したので、以下、英文での記載とする。

Background

Search for new energy sources becomes an urgent challenge in our society and is greatly related to the technology development. Such energy requires high efficiency, convenient, pollution-free and safety. As alternative energy sources and energy storage media, batteries have many advantages and are principle and promising power sources for a wide variety of electronics, e.g., portable, entertainment, computing and telecommunication equipments, as well as electric vehicles (EV) and hybrid electric vehicles (HEV) [1]. A typical battery is composed of many electrochemical cells in series in terms of exporting-energy requirement. Single cell contains a positive electrode (cathode) and a negative electrode (anode), which are separated by an ionic-conducting but electron-insulating electrolyte. The working voltage of the cell is due to the potential difference between the cathode and the anode (both sources of chemical reactions). Furthermore, the chemical reactions processed in both cathode and anode can generate electrons and currents in case of an external circuit connection between the two electrodes. The amount of electrical energy produced by the battery is dependent on several key parameters such as working voltage (V) and specific capacity (Ah Kg^{-1}), both of which are linked directly to the chemistry of the system, and is expressed according to either per unit of weight (Wh kg^{-1}) or per unit of volume (Wh L^{-1}). At present, fuel cell, nickel metal hydride and lithium ion batteries are the major research and attract even-increasing attention. In particular, lithium ion batteries have a remarkable expansion and now supply over 63 % of the total portable battery market in worldwide (90% in Japan, data cited from 2001) [2]. This is attributed to that lithium ion cell has rather high working voltage and thus large energy density. There is a long historical development over 30 years for Li-battery technology. The initial motivation for using Li as anode in batteries is due to the fact that metallic lithium possess the most electropositive character (-3.04 V vs. standard hydrogen electrode) and the lightest weight (equivalent weight M= 6.94 g mol^{-1}, specific gravity ρ=0.53 g cm^{-3}), as well as the largest capacity density (ca. 3.8 Ah Kg^{-1}); thereby battery based on lithium anode shows very high discharge voltage and correspondingly large energy density. However, lithium dendrites that occur on the surface of the lithium anode during the repeated charge and discharge tend to cause a short current circuit and thereby a potential safety problem. Fortunately, this deterrent was tackled successfully by Sony Corporation, Japan, in June 1991, by introducing a

kind of Li-intercalation host, such as graphite, in place of metallic lithium. Correspondingly, lithiated $LiCoO_2$ (lithium cobaltate) is adopted as cathode that gives high potential and acts as Li-sources. The "rocking chair" concept of the lithium ion cell proposed and commercialized firstly by Sony Corporation, as shown in Fig.1, make mobile Li^+ become shuttle between the cathode ($LiCoO_2$) and the anode (graphite) via the electrolytes in a charge and discharge process accompanied with an electrochemical electrode reaction. During the charging process under an applied external voltage, a certain amount of Li^+ are extracted from the cathode into the electrolyte, which is composed of lithium salt dissolved in a liquid solvent or a solid polymer/glass and is not consumed by the electrochemical charge–discharge reaction. Simultaneously, an equivalent amount of lithium ion are forced from the electrolytes intercalate into the graphite anode. The movement of the lithium ion during discharge is reverse to that of charge stage and is spontaneous. Charge compensation takes place through the external circuit during charge and discharge. By this way, the electrical energy can be saved during charging and released during discharging reversibly. The "rocking chair" manner highly avoids Li-dendrites and thus demonstrates high reliability. The currently commercial lithium ion cell consisting of $LiCoO_2$ and graphite has high discharge voltage of ca. 3.7 V and large energy density of ca. 110 Wh Kg^{-1}, which are apparently superior to those of Ni-Cd and Ni-MeH cells. Obviously, electrode materials that can reversibly storage lithium ion are the key for developing further lithium ion batteries. The research in the cathode that must possess high electrode potential mostly focuses on how to improve the electrode capacity, which is below to 200 mAh g^{-1} in the current system, indicating that the weight of cathode to anode must be over 2 times. The large efforts have resulted in series new compounds such as layered mixed transition metal (Ni-Mn-Co) oxides (e.g., $LiNi_{1/3}Co_{1/3}Mn_{1/3}O_2$) [3] and olivine lithium iron phosphate (e.g., $LiFePO_4$) [4], which appear to be promising cathode alternatives for $LiCoO_2$ and is in the stage of application. In the anode side, research remains more urgent, although various exotic carbonaceous and non-carbonaceous materials, e.g., disordered carbon [5], Li-alloys [6], lithium transition metal nitrides [7], transition metal oxides [8] and composite tin oxides [9], have been deeply studied with an improved capacity. It means that the "standard" carbonaceous materials, such as graphite and coke, are still likely to be the anode of choice for the next few years. A considerable investigation in our group for developing further Li-ion batteries has been under progress over 10 years and has lead to some remarkable results including of the electrode materials, the electrolytes and the battery system. In this paper, we give a brief introduction of the anode research of recent two years. Especially, the synthesis, characterization, electrochemical behavior and safety problem of these novel anode materials are discussed and

presented in detail according to the types of electrolytes, such as liquid organic electrolytes and solid polymer electrolytes.

Long time

Part I: Liquid electrolytes based system
1. Li-alloy based composites

1. Introduction

Electrode material is a key for developing further lithium ion batteries, which are likely to require good reliability and high energy density[10]. There is even-increasing research in the feasibility of the replacement of graphitic anodes currently used in commercial Li-ion battery. Numerous metals, e.g., Mg, Ca, Al, Si, Ge, Sn, Pb, Sb, Bi, etc., can reversibly accommodate lithium under an electrochemical alloying process according to the mechanism: $xLi^+ + e^- + M = Li_xM$, resulting in larger theoretic specific and volumetric capacities[11]. In general, Li-alloys have several advantages over lithiated graphitic (LiC_6) materials which favor their use in a Li-ion cell, including of higher lithium storage capacities, in particular, when the charge densities are comparable to metallic lithium, and a relatively higher operating voltage, retarding the deposition of metallic lithium during charge, and thus improving safety and fast-charging capability. Besides, Li-alloys appear not to have much sensitive to the solvent co-intercalation compared with the graphitic anode materials. However, there is a major problem that encumbers the application of Li-alloys, as that the volume mismatch of the alloy hosts between Li intercalation and extraction is comparatively large (typically in the scale of over ca. 200 %), and such that the host matrix undergoes drastic mechanical stresses during charge and discharge leading to the electrical contacting loss from the host particles, and thus capacity fading. Recently, we pay our attention on silicon, which has a low reactive potential of ca. 0.2 V vs. Li/Li^{-1} and the highest capacity of ca. 4000 mAh g^{-1}, which is 10 times as that of the current graphite, among all known lithium storage hosts. In this work, we report some recent results upon the development and mechanism studies of such type anode for Li-ion batteries.

2. Structural and morphological changes of Si upon electrochemically Li-alloying process

There have been some reports revealing that a large amount of Li$^+$ can be electrochemically intercalated into silicon and crystalline structure of Si may changes with growing dose of inserted lithium ions[11-14]. For example, Li et al[15] reported that the crystals of Si were destroyed due to

the insertion of a large amount of Li^+ leading to the formation of an amorphous structure. They observed a possible re-crystallization from the electrochemically driven amorphous Si upon Li-extraction. However, there is still lack of clarity for micro-structural change of Si relating to the evolution from crystal to amorphous upon Li insertion and extraction and the reversibility of such a Li-alloying process. In this work, two kinds of Si particles of $\leq$ 1 µm and 60 nm were chosen and investigated via ex-situ Raman, XPS, XRD and HRTEM.

Fig.2 shows structural changes of the crystalline Si upon different charge and discharge depth. The crystalline reflection from starting Si gradually decreases upon Li intercalation and finally disappears under a heavy Li-accumulation ($Li_{22}Si_5$), indicating a phase transformation from crystal to amorphous. Such a structural change appears to be irreversible upon Li-extraction while a heavy Li-intercalation (e.g., <50 mV vs. Li/Li^+, or $Li_{13}Si_4$) occurs. However, Raman spectra confirmed that a re-crystallization from the electrochemically driven amorphous Si is highly available and does not depend on the Li-insertion levels. XPS measurements shown in Fig.3 further unveils that chemical bonding energy of the starting Si (Si 2P3/2) gradually grows upon Li insertion, and then drops back upon Li-extraction and close to that of the α-Si. Compared with pure Si (in both amorphous and crystalline stages), the electrochemically Li-alloying reaction make chemical bonding energy of the Si (Si 2P3/2) increase and remain under a high level even after Li-extraction, probably due to that still some of the inserted Li could not be reversibly extracted. Such a bonding effect from Si which may attract Li^+ appears to be very strong and does not depend on the Li-insertion degrees. Furthermore, we use high-resolution transition electron microscopy (HRTEM) to directly observe the micro-structural change of Si upon Li insertion and extraction, as shown in Fig.4a-d. The image of the crystalline bulk Si ($\leq$1µm) is shown in Fig.4a in which perfect (111) layered lattice fringes can be seen in the selected region. Such a structural character also can be observed to the Si particle of 30-80 nm. Under a heavy Li-insertion ($Li_{22}Si_5$), the (111) layered lattice fringes of crystalline Si (30-80 nm) entirely disappears and is completely replaced by an amorphous structure, as shown in Fig4b, indicating that the insertion of Li^+ destroys the crystals of Si directly instead of formation of any intermediate phases. With further complete Li-extraction, Si atom tends to form many small domains of 10-15 nm in an onion structure, as shown in Fig4c, probably due to the Si-atom rearrangements and amalgamations which are motivated by the mechanical stress in a repeated volumetric expanding/shrinking process. As can be seen, structure of the innerness of the Si-domain still is prevailed with amorphous and that of the outer layers has some lattice fringes which are similar but still different from the starting crystalline Si and possess porous characteristics. Such an inhomogeneous phase distribution within the small domain

probably is due to that the penetration speed of Li$^+$ and the bonding energy of the Li-Si between the inner grains and the outer layers could be different. As observed, structural change from Si particle of ≤1 um possesses a similar behavior. However, due to an enlarged inhomogeneity of both electrical contact and concentration distribution of Li$^+$ in a relatively wide region, the phase transformation and distribution could be very inhomogeneous, as shown in Fig.4d, in which a lot of the amorphous regions were also observed besides the re-crystallization regions.

The electrochemical behaviors of Si with different particles (e.g., 200, 10, 4, ≤1 μm and 60 nm) were further investigated. All Si is reactive to lithium resulting in large capacities. However, all Si suffers from poor capacity retention after several initial cycles. This can be attributed to several reasons including of such as: a) decrease in the active hosts still is insufficient (unless < 10-15 nm, defined as the smallest reactive region which can avoid a possible morphological instability), b) lack of a feasible contact between the electron-channels and the semiconductor Si, and c) difficulties in obtaining an electrode with highly homogeneous Si-distribution. In fact, due to the extreme difficulties of direct utilization and preparation for the active bulk-Si with ultrafine size and high purities, a feasible structure via easy preparation should be required in order to motive the Si as high capacity anode for commercial Li-ion batteries.

3. Design a suitable structure consisting of active Si and conducting phase

3.1 Preparation of the Si/C composites using different Si particles

There are many reports relating to the designs to overcome the capacity-fading dilemma of Si[16]. In particular, the Si/C composites proposed from dispersing polycrystalline Si (from nano- to micro-) within a conducting carbon via thermal pyrolysis have attracted much interest[17,18], because of several advantages such as high Si-capacity utilization, high 1st cycle efficiency, a noticeably improved cycling stability, and especially, easy process ability, e.g., in comparison with the Si/C composites prepared by thermal vapor deposition[19,20,21] As can be seen in Fig.5, a suitable reversible capacity of such a Si/C composite can be chosen based on Li-intercalation levels and Si contents while the effects from the pyrolyzed carbon (e.g., capacity and 1st cycle efficiency) are fixed.

As discussed, to diminish the volume effects from active host, decrease in Si particles to nano-scale or below is highly necessary. However, such a Si particle seems be conflict with its utilization and preparation. Thus, we firstly pay our intention on preparing the Si/C composites with different starting Si over nano-scale. For example, in case of Si of ca.1 μm, we proposed a Si-C composite from two poly (vinyl chloride) (PVC) pyrolysis reactions, combined with an intervening

high-energy mechanical milling (HEMM) step. The intention of the intervening HEMM step is to decrease the active Si size, increase the Si-distribution, and further improve the contact between the pyrolyzed carbon and the Si. Such a composite shown in Fig.6 presents a large capacity of 900 mAh g^{-1}, high initial charge efficiency of 81%, and an average potential of 0.25 V. However, still a small potential hystersis of about 0.2 V between the charge and discharge is apparent. The electrochemical behavior of the Si/C composite is dominated by Si insertion-host, suggesting only small amount Li storages in the carbonaceous matrix. Furthermore, we proposed several Si-M-C composites by ballmilling relatively hard components (M, such as fine powers of graphite, TiB$_2$, TiC, and TiN etc) with normal Si (average starting particles $\geq$ 1um), and then carrying out a pyrolysis process in presence of PVC. The introduced co-milling components (M) bring an increase in the charge rate and cycling stability over the Si-C composite (Si at ca.1μm), due to a significant decrease in the active Si size (to be 0.1 nm or below). As shown in Fig.7, the capacity retention at the 35th cycle of the Si-C composite was ca. 80%, vs. ca. 900 mAh g^{-1} at the second cycle, while for the Si-M-C composites, the capacity of ca. 600 mAh g^{-1} in the second cycle was remained to over 90% at the 35th cycle. However, the introduced co-milling component leads to a slight loss in the capacity utilization for active Si. XRD measurements conducted on the ballmilled Si-M (M as conducting TiN, TiB, TiC etc) shown in Fig.8 reveals that crystalline reflection from Si suffers from a loss in association with the milling time, while a new active SiM phase does not appear. Our research reveals that both electrochemical and mechanical reaction may decrease Si size and make Si amorphous while the latter has a propensity in losing electrochemical activity due to the molecular-interaction changes of Si. It suggests that choosing a suitable matrix to compatible with Si via the mechanical milling is necessary. For example, Matsushita group reported using Ti, instead of TiN, TiC, graphite, treat the active Si to obtain a composite with a relatively high Si-capacity utilization and good cycliability[11]. Furthermore, in spite of its cost, we proposed the Si/C composites by direct using nano-Si (e.g., in 60 nm, as prepared) as active hosts. In such case, co-existing of suitable carbonaceous fillers with a high porosity and large surface was found to be very favorable for the Si distribution and the contact between Si and carbon. The cycling performance of such a Si/C composite is highly superior to that of pure nano-Si, as shown in Fig.9. However, the low 1 st cycle efficiency seems to be unavoidable in comparison with the Si/C or Si/M/C composites discussed above, due to the high impurities from the nano-active Si itself.

3.2 Function of the pyrolyzed carbon

The enhanced cyclability of the Si/C composite over pure Si is attributed to the small volume

expansion of carbon on lithium intercalation (ca. 9% for graphite) and the ability of the ductile carbon to accommodate the volume change of silicon, reducing mechanical strain within the electrode and consequent electrode disintegration. Although this type of pyrolyzed carbon has a potential hysteresis between Li insertion and extraction, it may mostly function as an elastic network with electron/ion conductivity that permits the silicon in the carbon matrix to operate while maintaining electrode integrity. There are several factors that influence the electrochemical behavior of the Si/C composites, e.g., the morphology of Si (i.e., particle size, distribution, and structure), the construction/texture of the pyrolyzed carbon (i.e., porosity, ductility), and the interfacial contact between the active Si and the conducting carbon. In general, influence from particle size upon cycling stability of the Si has been well known and widely discussed in many references. Here, we may pay more attention on the Si/C interface according to several considerations: 1) a lot of impurities that are composed of silicon oxide, micro-twins, stacking faults and low-angle grains can always co-exist on surface of the polycrystalline Si as prepared, leading to a low 1st cycle efficiency and poor Li-diffusion and electron contact; 2) mechanical stress at the Si/C interface caused by the volume effect from Si tends to break the electron-contacting; and 3) a good conducting channels are supposed to be highly necessary due to the semiconductor Si characteristics.

Fig.10 shows XRD patterns of the Si/C composite based on different carbonaceous precursors. All the reflected peaks correspond to the crystalline Si, excluding of that from Si-PVDF, which has an inert SiC phase. The comparison shown in Fig.11 further reveals that the carbon matrix has an obvious effect upon the cycling performance of Si/C composites. We found that such a electrochemical cycling stability of the Si/C composites does not depend on some characteristics from the pyrolyzed carbon, such as H/C ratio, carbonized production, loading density, disordered/graphene (D/G) peak area ratio (in Raman spectrum), and electric conductivity. In addition, porosity from the Si/C composites could be similar under controlling the heating rate. Therefore, we attributed such a difference in the cyclability to the interfacial performance between Si and carbon. As confirmed with XPS, carbonaceous precursors containing elementals such as F and Cl can clean surface impurities of Si, resulting in an improvement of electrochemical behavior. Fig.12 further shows the weight of the Si-PVDF mixture suffers from an obvious loss during heating process while those from Si and carbon remains stable under the same temperature, indicating that the surface-effect occurs at a relatively low temperature before the carbonaceous precursors decompose. A good interface shown in Fig.13 of such a Si/C composite might result in an improvement in the electric conductivity for the semiconductor Si and holds a stable conducting channel for the Si upon Li insertion and extraction.

3.3 Limitation of the Si/C composite

The Si/C composite presents a promising way to conquer the cycling instability of Si. Controlling Li insertion level may effectively improve the morphological stability of the Si/C composites, due to the alleviated disintegration and deactivation from Si. Meanwhile, reducing the Li-insertion degree may suppresses Si degradation on cycling. However, as observed, still capacity fading occurs upon the extremely extended cycles even under different testing conditions. The reason appears to be complicate. A SEM analysis with respect to the Si/C composite under various charge-discharge cycles unveiled such capacity decay. Compared with Fig.14a (before cycling), many micropores (1~2 μm) become visible on the surface of the materials at the 35th cycle, as shown in Fig.14b. With cycling, the micropores obviously turn into enlargement (2~4 μm at the 200th cycle), as shown in Fig.14c. Since Si suffers from a rearrangement and amalgamation and tends to form small regions of 10-15 nano-scale upon Li-intercalation and extraction, such a structural change causes to a seriously mechanical instability while the active Si in the Si/C composite is in a range of > 10-15 nano. Gradually, it leads to a) form porous structure within the carbon matrix due to the breathing effect from Si (volume change), b) pulverization of Si, c) a possible electrical disconnection at the Si/C interface, and d) more Li being attracted. On the other hand, the penetration of the electrolytes within the composites through the micropores could speed the disconnection as a consequence of a direct contact of Si with the electrolytes. Impedance measurement upon the Si/C composite also reveals that fresh area of the Si/C composite appears and exposes to the electrolytes upon cycles. It suggests that the active Si within the conducting carbon still is one major factor dominating a long-term cycling stability.

3.4 A novel Si/C structure

Based on above observations, we developed a novel amorphous structure, in which active Si (in several nano-scale) are highly dispersed in an inert Li_2O matrix and further embedded with a conducting carbon[11]. Firstly, we prepared a $Si-Li_2O$ composite using SiO and Li as staring materials according to the reaction of $SiO+Li \rightarrow Li_2O+Si$ via high energy mechanical milling by aids of an organic solvent. Fig.15 shows phase changes of composites based on SiO via different treatment. It indicates that active Si could be in situ obtained from SiO. Fig.16 shows charge and discharge profiles of the $Si-Li_2O$ as prepared. Differing from SiO which suffers from a large capacity loss at the first cycle (1st efficiency: ca. 44%) due to the irreversibly electrochemical reaction of

$Li^+ + SiO + e^- \rightarrow Li_2O + Si$, the Si-Li$_2$O composite shows high first cycle efficiency (close to 90%) since its electrochemical reaction starts directly from the Li-Si alloying process. The Li$_2$O-Si composite has a good cycling stability, which is comparable to SiO$_x$ as shown in Fig.17. Fig.18a-c unveils that the formed active Si is in nanocrystalline (1-3 nm) and highly dispersed in the inert amorphous Li$_2$O matrix. There is no phase boundary between Si and Li$_2$O indicating a very good Si-Li$_2$O interface. However, Li$_2$O was found to be obstructive to the Li-Si alloying reaction due to its poor electrical conductivity. Therefore, the Si-Li$_2$O was embedded with a conducing carbon via the PVC pyroysis reaction. The Si-Li$_2$O/C shows a relatively high reversible capacity of about 600-700 mAh g^{-1}and excellent capacity retention compared with the Si/C composite proposed above. According to analysis, such an excellent cyclability probably is attributed to several factors as 1) extremely low volume change from single Si; 2) good Si distribution and good conducting interface; 3) conducting and feasible matrix which can absorb the volume effects from Si. However, carbon coating was found to bring an apparent decrease in the first cycle efficiency for the Si-Li$_2$O composite. In addition, the process for the Si-Li$_2$O appears to be difficult for large scale preparation. Therefore, understanding and improvement upon such material still is under progress.

4. Conclusion

1) The electrochemically driven amorphous Si could be partly re-crystallization with Li-extraction and still part intercalated Li$^+$ can not be extracted reversibly. During the volumetric expanding/shrinking process, silicon tends to form small regions of <10-15 nano- in an onion structure. It indicates that particle scale of Si lower than 10-15 nm may essentially avoid the morphological instability upon cycles.

2) Si/C composite proposed by thermal pyrolysis possesses a promising way to tackle the capacity fading of Si. We show several designs using normal Si in different particles via feasible and easy preparations. The major factors influencing the electrochemical characteristics of such Si/C composites were investigated and discussed. Carbon precursors containing elementals such as F, Cl, can clean surface impurities of Si, resulting in a good Si/C interface and therefore an improvement in the electrochemical behavior. However, still the active Si is the major factor dominating a long-term cyclability.

3) Furthermore, a promising structure is suggested and investigated.

2. Lithium transition metal nitrides based composite electrodes

2.1 Introduction

In view of the morphology stability, especially, under high Li-utilization, lithium transition metal nitrides with hexagonal symmetry, P6/mmm, such as $Li_{2.6}M_{0.4}N$ (M=Co, Cu, Ni), are superior to Li-alloy in the cyclability as promising anode candidates. The ternary $Li_{2.6}Co_{0.4}N$ is composed of Co substituting lithium between the $Li_2^+N^{3-}$ layers of Li_3N. Li_3N has two kinds of Li ion. That is, location (1): Li ion is located in the Li_2N layer and (2): Li ion is located between the Li_2N layers. It is believed that Co substitutes Li ion in the location (2), as shown in Fig.19. The intercalation mechanism of the layered lithium transition metal nitrides has been primarily investigated by this group and T. Shodai et al. [7,22-26]. The solid solution range of the $Li_{3-x}M_xN$ is located in 0<x<0.5, 0<x<0.6 and 0<x<0.3 for M=Co, Ni and Cu correspondingly. From an electrochemical standpoint, the most promising and most studied of the compound in this family is $Li_{2.6}Co_{0.4}N$. It was found that the large capacity of 900 mAh g^{-1} of $Li_{2.6}Co_{0.4}N$ is associated with a structure change from a crystal to an amorphous phase in the first Li-extraction process [25]. Such a transformation indicates the atom rearrangement and lithium in the compounds can be electrochemically extracted and re-intercalated with high reversibility. However, $Li_{2.6}Co_{0.4}N$ does not show satisfactory capacity retention upon long cycles. The capacity fading is attributed to the electrochemical instability under high Li-extraction and the interfacial incomparability on the surface of the active hosts [27,28]. In the pervious work, we have developed a series co-doped lithium transition metal nitrides by means of combination of solid-state reaction at high temperature and high-energy mechanical milling (HEMM) process [29]. These compounds are superior to ternary $Li_{2.6}Co_{0.4}N$ in terms of capacity retention and cost. On the other hand, lithium must be extracted from the nitrides in an initial anodic oxidation, indicating that these Li-rich type anodes cannot directly combine with the typical high potential cathodes such as $LiCoO_2$ and $LiMn_2O_4$ to make Li-ion cells. We have showed that the Li-rich compounds can be used as insertion hosts in several ways. For example, lithium in the compounds can be pre-extracted by a chemical way before assembling a cell [30]. Lithium metal nitrides also can be introduced to make compensation for the irreversible capacities of the alloy, carbon and metal oxides based electrodes in the first cycle [31-33]. Furthermore, we designed a type of Si-graphite-$Li_{2.6}Co_{0.4}N$ composite via two HEMM steps [34]. Due to the capacity compensation from the lithiated $Li_{2.6}Co_{0.4}N$ in the first cycle, the composite material demonstrates an extremely high initial faradaic yield of 92%, as well as a large capacity and an acceptable cyclability. Recently, we have reported a composite electrode consisting of spinel $LiTi_2O_4$ and lithium metal nitrides. $LiTi_2O_4$ can extract lithium from the lithium transition metal nitrides and function as an inert-conducting material in the electrodes within a special potential range [35]. The composite electrode shows high volumetric capacity and excellent cycling stability. More recently, we found that the novel composite anodes, which consist of transition metal oxide, such as Co_3O_4, and hexagonal lithium transition metal nitrides, demonstrate high electrochemical capacities of about 500

mAh g^{-1} and 100 % capacity retention at the first cycle, as well as good cyclability [36]. Transition oxides can thermodynamically extract lithium from the lithium transition meal nitrides that leads to a delithated state of the nitrides and to form metallic Co and Li$_2$O. Thus, lithium transition metal nitrides can be directly treated as being in a delithiated state. Such a composite anode also shows high interfacial compatibility and low reaction heating with solid PEO electrolytes. In this part, some of the above obtained results based on the hexagonal lithium transition metal nitrides are presented and discussed in detail.

2.2 Experimental

2.2.1 Materials preparations and XRD measurements

The hexagonal compound was prepared by a solid state reaction following a pervious report [22]. The basic procedure was as follows: mixtures of Li$_3$N and powders of transition metal were pressed into tablets with 8 mm in diameter and 5-8 mm in thickness in an Ar atmosphere. The tablets were heated at 700°C for 12 h under a N$_2$ stream at a heating rate of 35 °C min^{-1}. The reactions were allowed cool down to room temperature normally. For the compounds containing Fe, heating temperature was increased to 800 °C. The resulting products were ground in a glove box and further treated by high-energy mechanical milling (HEMM) at a rotational speed of 500 rpm for 20 h. Powder X-ray diffraction (XRD) patterns were obtained using automated powder diffractometer with Cu K$_\alpha$ radiation (Rotaflex RU-200B, Rigaku-denki Corporation). The samples assembling and measurements were performed under air-sealing condition.

2.2.2 Electrode fabrications and electrochemical measurements

A given weight of the electrode components, including 20 wt% acetylene black (AB), 70 wt% active materials and 10 wt% Poly (vinylidene fluoride) (PVDF), was homogeneously mixed in an agate mortar in a glove box and further pressed onto a 300-mesh stainless steel grid, which served as a current collector. The geometric area of the electrodes was 0.55 cm^2, and the typical thickness was 100~160 μm. Electrode capacity was calculated according to the weight of active materials. To evaluate the electrochemical properties of the electrode, a half-cell containing LiPF$_6$ / EC+DMC (Ethylene carbonate plus diethyl carbonate as 1:1 in volume) electrolytes was used. Li metal was utilized as both the counter and reference electrode. The structure of such a cell is similar to that of Si based cells. Basically, all the three layers, including test electrode, separator and Li metal, were stacked in a 2025 coin type cell in a glove box. Unless stated elsewhere, cycling was started from discharge and carried out at a potential cutoff at 1.4/0.01 V and a constant current density of 0.15 mA cm^{-2}. The rest time between charge and discharge was 1 min. Charge and discharge of the cell refer, respectively, to lithium extraction from, and insertion into, the active hosts. The impedance response was measured with a Solartron SI 1260 (impedance / gain-phase analyzer) in a frequency range from

0.1 to 10^6 Hz.

2.3 Results and discussion

2.3.1 The doped elementals upon the electrochemical behavior of the ternary $Li_{2.6}Co_{0.4}N$

The composition of the resulting compounds is confirmed by Inductively Coupled Plasma (ICP). Fig.20 shows X-ray diffraction patterns of the prepared lithium transition metal nitrides. The XRD responses are well in accordance with those of $Li_{2.6}Co_{0.4}N$ recorded on JCPDS card 5-605, indicating a typical hexagonal structure, isostructural with Li_3N, in which part of lithium in Li_3N is substituted by Co, Cu, Ni or Fe. No impurity phase, such as Li_2O, residual Li_3N and metals, can be detected. The collected lattice parameters of the hexagonal compounds are shown in the inset in Fig.20. Due to the atom radius of the doped metals, $e.g.$, Ni<Co<Cu, the a-axis gradually decreases from $Li_{2.6}Ni_{0.4}N$ to $Li_{2.6}Co_{0.4}N$, until $Li_{2.6}Cu_{0.4}N$. As a result, the affinity between the Li-M (M=Cu, Co, Ni) layer (2) and the Li^{1+}-N^3-Li^+ layer (1) is decreased with the increasing of the affinity within the Li^{1+}-N^3-Li^+ layers (1). The a-axis increases again in the range from $Li_{2.6}Cu_{0.4}N$ to $Li_{2.6}Ni_{0.4}N$. The c-axis is changed along with the opposite direction of a-axis. When Co content is 0.2, both a and c axis show the largest value in the case of Co, Cu and Ni coexist.

As found, the electrochemical behavior of the $Li_{2.6}Co_{0.4}N$ is superior to those of $Li_{2.6}Ni_{0.4}N$ and $Li_{2.6}Cu_{0.4}N$. To keep the charge balance of $Li_{2.6}Co_{0.4}N$ upon oxidation and reduction state, both cobalt and nitrogen play an important role. Fig.21 shows charge and discharge curves of the selected 1) $Li_{2.6}Co_{0.4}N$, 2) $Li_{2.6}Co_{0.2}Cu_{0.2}N$, 3) $Li_{2.6}Co_{0.2}Cu_{0.1}Ni_{0.1}N$ and 4) $Li_{2.6}Co_{0.2}Cu_{0.15}Fe_{0.05}N$ electrodes at different cycle. Due to the vacant sites introduced by the existence of Co^{2+}, the fully lithiated nitrides still permit small amount of lithium intercalation into in the first cycle, as shown in Fig.21a. The compounds gradually undergo an irreversible transformation from a crystal to an amorphous phase in the initial Li-extraction stage, resulting in the noticeable potential plateaus at 1.0, 1.2, 1.1 and 1.1 V for $Li_{2.6}Co_{0.4}N$, $Li_{2.6}Co_{0.2}Cu_{0.2}N$, $Li_{2.6}Co_{0.2}Cu_{0.1}Ni_{0.1}N$ and $Li_{2.6}Co_{0.2}Cu_{0.15}Fe_{0.05}N$, respectively. Compared with $Li_{2.6}Co_{0.4}N$, the obvious increases of $Li_{2.6}Co_{0.2}Cu_{0.2}N$, $Li_{2.6}Co_{0.2}Cu_{0.1}Ni_{0.1}N$ and $Li_{2.6}Co_{0.2}Cu_{0.15}Fe_{0.05}N$ in the charge potentials indicate that part Co substituted by Cu, Ni and Fe may be obstructive to the lithium extraction. At the fifth cycle, the $Li_{2.6}Co_{0.4}N$ and $Li_{2.6}Co_{0.2}Cu_{0.15}Fe_{0.05}N$ electrodes as shown in Fig.21b have a small potential fluctuation at $ca.0.9$ V and 1.3 V in the Li-extraction stage. This consequence is related to an atom rearrangement associated with the doped elementals, Li and N.

Cycling comparison reveals that the co-doped compounds have a remarkably enhanced cyclability, as shown in Fig.22. By optimizing the tradeoffs for capacity and cycling in accordance with the ternary $Li_{2.6}M_{0.4}N$, we have confirmed that the appropriate compositions in this family should be in the range, which can be stated by a formula as $Li_{2.6}Co_{0.4-x-y}Cu_xNi_yN$ ($0.1 \leq x \leq 0.2$, $0 \leq y \leq 0.1$, $0.1 \leq x+y \leq 0.2$). Furthermore, a certain amount of doped Fe was found to increase the capacity and is in

favor for the cycling. Compared to $Li_{2.6}Co_{0.4}N$, the obviously improved cyclability of the co-doped compound may be partly attributed to the enhanced interfacial compatibility between the active particles and the electrolytes. The inset in Fig.22 shows Cole-Cole plots of the impedance response of $Li_{2.6}Co_{0.4}N$ and $Li_{2.6}Co_{0.2}Cu_{0.2}N$ electrodes with the delithiated stage vs. Li after 30 cycles. With part Co substituted by Cu, the total resistances of the half cell significantly turn into lessen, resulting in not only an improved interfacial compatibility, but also an enhanced capacity retention. In addition, according to the capacity utilization in $Li_{2.6}Co_{0.4}N$ and $Li_{2.6}Co_{0.2}Cu_{0.2}N$, the comparatively low Li-extraction level in $Li_{2.6}Co_{0.2}Cu_{0.2}N$ is favorable for the cycling stability. We have observed that the capacity fading of the ternary $Li_{2.6-z}Co_{0.4}N$ can be effectively suppressed if the Li-extraction is limited at $z \leq 1.0$.

To further unveil the reliance of the electrochemical behavior upon the structure change along with Li-extraction, the variation of the lattice parameters of $Li_{2.6-z}Co_{0.4}N$ and $Li_{2.6-z}Co_{0.2}Cu_{0.2}N$ with various charge-discharge depths in the scale of $0<Z<1.0$ in the first Li-insertion/extraction process was measured and shown in Fig.23. The pointed sites of a~e in a_1 and b_1 indicate the special Li-insertion/extraction stage while the corresponding lattice parameters are shown in a_2 and b_2. In the charge process, it is obvious that the a-axis decreases with the c-axis increases, relating to the composition range where the potential gradually increases to 1.0 V for $Li_{2.6}Co_{0.4}N$. Above $z\sim0.3$, no remarkable change in the cell parameter is observed until $z=1.0$, but decline in the XRD responses peak turn into noticeable. It suggests that the Li-extraction is associated with the two-phase reaction and the crystalline structure finally becomes amorphous. In the case of $Li_{2.6-z}Co_{0.2}Cu_{0.2}N$, the slight decreasing of a-axis along with the increasing of c-axis occurs much early, and there is no change in the lattice parameter above $z\sim0.2$. However, we notice that the crystalline response peaks, which are linked to the phase transformation, apparently reduce. It indicates that the formation of an amorphous phase appears in the very early charge region. As a result, lithium extraction from the $Li_{2.6-z}Co_{0.2}Cu_{0.2}N$ becomes difficult, leading to a decreased capacity compared to that of the $Li_{2.6-z}Co_{0.4}N$.

2.3.2 The effects of the morphology performance upon the electrochemical behavior

Morphology performance of the particles after was found to show obvious effects upon the electrochemical behavior. Fig.24 shows charge and discharge curves of $Li_{2.6}Co_{0.2}Cu_{0.2}N$ without and with HEMM. The initial insertion capacities were significantly enlarged when the particles were treated under HEMM for 20h. Compared with the un-milled samples, the milled nitrides had an obviously decreased ratio of Li vs. doped elementals from the ICP measurements. It appears to be related to the increased Li-free sites and the valance change of part Co. Thus, we assumed that HEMM enables the removal of part lithium in the Li-rich compounds. A decrease in the first extraction potential plateau probably is attributed to that HEMM make the crystalline lithium transition metal nitrides partly amorphous. The milled samples have an increased capacity and a

decreased Li-extraction potential. This can be explained by the reduced potential polarization arising from the improved electrochemical kinetics, e.g., the shorten lithium diffusion path and the improved interfacial charge transfer that relates to the enlarged reactive area of the insertion hosts. The HEMM alleviates the obstruction to the lithium extraction; thereby increases the Li-extraction degree at a certain extent. A comparable cycling stability of the milled lithium transition metal nitrides is available in accompany with a deep Li-extraction, as shown in the inset in Fig.25. However, the $Li_{2.6}Co_{0.2}Cu_{0.2}N$ directly synthesized by HEMM does not bring the same consequence. It is probably due to the incomplete reaction and poor atom distribution. We have observed a lot of residual Li_3N and transition metals in the XRD patterns for the sample prepared by HEMM. This means that high-energy mechanical milling step alone is insufficient for achieving the good crystalline formation for the multi-doped compounds.

2.3.3 Novel composite electrodes based lithium transition metal nitrides

1. Carbonaceous materials-lithium metal nitrides composites

MCMB is a kind of graphitic carbon and currently used as anode material in the commercial Li-ion batteries. The composite consisting of MCMB and $Li_{2.6}Co_{0.4}N$ was developed via HEMM. SEM observation on the composite reveal that after ballmilling the $Li_{2.6}Co_{0.4}N$ powders are severely smashed into nano- or submicro- scale, and dispersed and adhered compactly on the surface of the MCMB particles, as shown in Fig.26. Such morphology is favorable for the electrochemical kinetics of the $Li_{2.6}Co_{0.4}N$ particles by adopting MCMB as an appropriate electron-conductive matrix. MCMB has a low reactive potential at ca.0.1 V vs. lithium and a reversible capacity of 310 mAh g^{-1}. As compared, we can apparently observe the increased initial coulombic efficiency (100% vs.89%) and the increased reversible capacity (450 mAh g^{-1} vs.310 mAh g^{-1}) for the $Li_{2.6}Co_{0.4}N$-MCMB composite electrode, as shown in the inset in Fig.27. The high faradic yield in the first cycle is dependent on the extraction capacity compensation of $Li_{2.6}Co_{0.4}N$. Compared with MCMB, the composite has a relatively enhanced safety due to the improved reactivity potential. The potential trends of the composite electrode reflect the mixing potential characteristics of these two types of active hosts. During cycling the $Li_{2.6}Co_{0.4}N$ yields charge potentials mainly in the realm of 0.6-1.1V vs.Li/Li$^+$ and discharge potentials of 0.15-0.5 V vs.Li/Li$^+$. As a result, an obviously potential hystersis of the composite electrode between charge and discharge is still remarkable. Fig.28 shows the cycling performance of the electrodes based on the MCMB-lithium metal nitrides composite and the pure MCMB. The capacity-cycle curves deliver high stability, indicating a high reversibility of Li-insertion and extraction.

2. Si-C-$Li_{2.6}Co_{0.4}N$ composites

Fig.29 shows charge and discharge profiles of the Si-graphite-$Li_{2.6}Co_{0.4}N$ composite synthesized from two HEMM processes. In the first discharge, the electrochemical behavior of the

composite is only associated to silicon and graphite because fully lithiated $Li_{2.6}Co_{0.4}N$ has no extra vacancy for the initial Li intercalation. The capacity above 0.8 V from $Li_{2.6}Co_{0.4}N$ plays an important role for the compensation for the irreversible capacity. As a result, a high first-cycle efficiency of ca. 90 % was obtained. From the second cycle to the subsequent cycles, the voltage trends show high coincidence that indicates a good reversibility of Li insertion and extraction. Moreover, graphite in the composite is favorable for reducing the potential hysteresis arising from silicon and $Li_{2.6}Co_{0.4}N$ in charge and discharge. An XRD measurement was further conducted on the composite with respect to various charge-discharge stages, as shown in the inset (1) in Fig.28. Before cycling, the diffraction peaks reflected from silicon, graphite and $Li_{2.6}Co_{0.4}N$ can be distinguished (see a). The diffraction peaks from silicon and $Li_{2.6}Co_{0.4}N$ disappeared with the first discharge and charge, as shown in b and c, respectively. The changed crystalline reflections remained same upon increasing of the cycle number. This result means that the electrochemical Li insertion and extraction make silicon and $Li_{2.6}Co_{0.4}N$ turn into amorphous. A SEM photo analysis reveals that all the components in the composite after HEMM tend to form large agglomerates, indicating that silicon could be highly dispersed and embedded within the ductile graphite–$Li_{2.6}Co_{0.4}N$ matrix. Obviously, such a granular structure is in favor for increasing the interfacial affinity of silicon with the matrix and leading to an ensured electrical contact. On the other hand, the low absolute volume effect of the composite using $Li_{2.6}Co_{0.4}N$ reduces the mechanical stress of the dispersed silicon. Thus, the composite demonstrates good cycling stability, as shown in the inset (2) in Fig.28. In comparison, silicon possesses the highest capacity of ca. 3.7 Ah g^{-1} in the first Li intercalation; but it suffers from a remarkable loss in the extraction capacity. By contrast, $Li_{2.6}Co_{0.4}N$ has a very low insertion capacity and very high extraction capacity. The Si–graphite–$Li_{2.6}Co_{0.4}N$ composite shows a large reversible capacity of ca. 1 Ah g^{-1} as three times as graphite and a high initial faradaic yield of 90 % that might lead to a high energy density of the lithium ion batteries.

3. LiTi₂O₄-lithium metal nitrides composites

The spinel $LiTi_2O_4$ demonstrates a high conductivity and an extremely constant charge/discharge potential versus lithium at ca. 1.55V, as well as a reversible capacity of ca. 170 mAh g^{-1}. The Li-intercalation potential of $LiTi_2O_4$ (ca. 1.50V) is slightly higher than the Li-extraction potential of $Li_{2.6}Co_{0.4}N$ (ca. 1.0V); therefore $LiTi_2O_4$ can extract lithium from $Li_{2.6}Co_{0.4}N$. Open potential of 0.95 V can be observed for the electrode when lithium in the $Li_{2.6}Co_{0.4}N$ was completely extracted. The suitable weight ratio of the nitrides to the $LiTi_2O_4$ in the electrode is dependent on the effective capacity and the molecular weight of the two active hosts. A possible chemical reaction between the two hosts is "$Li_{2.6-x}Co_{0.4}N + z\ LiTi_2O_4 \rightarrow Li_{2.6-x-z}Co_{0.4}N + z\ Li_2Ti_2O_4\ (x + z \leq 1.6)$", where x means the lithium loss in the $Li_{2.6}Co_{0.4}N$ compared to the theoretical Li:Co ratio as 2.6:0.4, and z is the possibly extracted lithium related to $LiTi_2O_4$. Thus, in view of the fact that the introducing of HEMM enables the removal of part lithium in $Li_{2.6}Co_{0.4}N$ and $LiTi_2O_4$ has no capacity contribution in

the electrode within a special potential range, the capacity utilization of the milled $Li_{2.6}Co_{0.4}N$ can be improved by reducing the contents of $LiTi_2O_4$. In the case of 22 wt% milled $Li_{2.6}Co_{0.4}N$ plus 70 wt% $LiTi_2O_4$, the first cycle efficiency is close to 100%. Fig.29 shows the charge and discharge curves of the electrode based on $Li_{2.6}Co_{0.2}Cu_{0.2}N$ and $LiTi_2O_4$ at different cycles. In general, a decreased particle size leads to an increased density. For example, the density of the mixture consisting of the separately milled $Li_{2.6}Co_{0.2}Cu_{0.2}N$ and $LiTi_2O_4$ is 3.2 g cm^{-3} according to the experimental data, versus 2.2 g cm^{-3} of the mixture based on the un-milled samples. Large volumetric capacity is dependent on the material's high specific capacity and density. In addition, $LiTi_2O_4$ can act as an inert-conducting additive in place of AB in the electrode within a potential range of 1.4V~0.01V vs.Li/Li^+. Thus, the composite electrode shows a comparative volumetric capacity. Taking $Li_{2.6}Co_{0.2}Cu_{0.2}N$ and $LiTi_2O_4$ as the active hosts, the volumetric capacity of the composite electrode is 798 mAh cm^{-3}, which is attractive compared to that of graphite (ca. 650-700 mAh cm^{-3}). The $Li_{2.6}Co_{0.2}Cu_{0.2}N$-$LiTi_2O_4$ composite electrode exhibits high cycling stability, as shown in the inset in Fig.30.

4. Co_3O_4-lithium metal nitrides composites

Fig.30 shows charge and discharge curves of the Li/Co_3O_4 (a), $Li/Li_{2.6}Co_{0.2}Cu_{0.2}N$ (b) and Li/Co_3O_4-$Li_{2.6}Co_{0.2}Cu_{0.2}N$ (c) cells. The Co_3O_4 electrode had a large insertion capacity of 1100 mAh g^{-1} along with a potential plateau of 1.1 V in the first cycle. However, its capacity retention at the subsequent cycle was below to 180 mAh g^{-1} within the potential range of 0.01-1.4V. The electrochemical behavior of $Li_{2.6}Co_{0.2}Cu_{0.2}N$ was in contrast to that of Co_3O_4, which had a high extraction capacity of over 800 mAh g^{-1} with a potential plateau of 1.1 V but a very low first insertion capacity of around 200 mAhg^{-1}. In contrast, 100 % capacity retention at the first cycle was observed in the Co_3O_4-$Li_{2.6}Co_{0.2}Cu_{0.2}N$ composite electrode. XRD studies of the Co_3O_4-$Li_{2.6}Co_{0.2}Cu_{0.2}N$ composite on different charged states, as shown in Fig.31, revealed that the diffraction peaks from $Li_{2.6}Co_{0.2}Cu_{0.2}N$ and Co_3O_4 disappeared by soaking the composite in the electrolyte for 2h. The diffraction intensities remained constant with increasing charge depth and number of cycles. These results indicate that a thermodynamically spontaneous reaction between Co_3O_4 and $Li_{2.6}Co_{0.2}Cu_{0.2}N$ leads to an amorphous delithiated state of $Li_{2.6}Co_{0.2}Cu_{0.2}N$ and probably to form metallic Co and Li_2O. We propose that the reaction mechanism of the composite anode as follows:

$$Li_{2.6}Co_{0.2}Cu_{0.2}N + xCo_3O_4 \rightarrow Li_{2.6-8x}Co_{0.2}Cu_{0.2}N + 4xLi_2O + 3xCo \qquad (1)$$

$$Li_{2.6-8x}Co_{0.2}Cu_{0.2}N + zLi^+ + ze^- \rightarrow Li_{2.6-8x+z}Co_{0.2}Cu_{0.2}N \qquad (2).$$
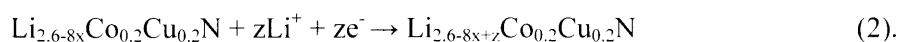
Reaction (1) is a chemical reaction and reaction (2) is an electrochemical one. If $Li_{2.6-8x}Co_{0.2}Cu_{0.2}N$ is the composition of the fully charged state, then reaction (2) becomes reversible during charge and discharge even at the first cycle. We estimated x and z as 0.16 and 1.7, respectively. These values correspond to 60/40 weight ratio of $Li_{2.6-8x}Co_{0.2}Cu_{0.2}N/Co_3O_4$ and the reversible capacity of 477 mAh g^{-1}. We observed a first charge and discharge efficiency of 100% and a reversible capacity of ca. 500 mAh g^{-1} for the composite anode of 62.5 wt % $Li_{2.6-x}Co_{0.2}Cu_{0.2}N$ plus 37.5 wt % Co_3O_4 as shown in

Fig. 32. The high first cycle efficiency proposed with this anode can greatly extend the capacity utilization for the cathode. It is remarkable because the capacity of the conventional cathode materials in lithium batteries is less than 200 mA g^{-1}. The irreversible anode capacity in the first cycle requires an extra capacity of cathode active materials; thereby it inevitably depresses the total energy density of the batteries. Due to lithium metal nitride as the active hosts, such a composite demonstrate excellent capacity retention with cycling, as shown in the inset in 23.

2.4 Conclusions

In summary, we have developed a series of lithium mixed transition metal (co-doped) nitrides with high electrochemical capacity and good cyclability. For producing these compounds, a combination of a solid-state reaction under an appropriate temperature and a high-energy mechanical milling step was involved. Research reveals that the granular structure of the nitrides shows obvious effects upon the electrochemical behavior. The lithiated compounds can be used in several ways to form new composite electrodes which demonstrate high insertion capacity, 100 % first cycle efficiency and excellent capacity retention ability. Therefore, they are promising anode candidates for further Li-ion batteries.

Part II Solid-state polymer electrolytes based system

1. Introduction

Since the discovery of ionic conductivity in the Poly (ethylene oxide) (PEO)-lithium salt composites, lithium-ion batteries based on such category of electrolytes has attracted worldwide attentions. In view of the high energy density and feasible design, all solid-state PEO rechargeable lithium batteries could be promising and ideal power source for EV&HEV [37]. So far, research has been extensively concentrated on two major points: the improvement of ionic conductivity of PEO-LiX complex at the relatively low temperature and the modification of interfacial characteristics between metallic lithium anode and polymer electrolytes. It is generally accepted that there is some instable issue between metallic lithium and PEO electrolytes caused by lithium dendrite grown [38,39]. Insertion hosts such as carbon, Li-alloy and Li-M-O, in place of lithium, present the promising alternative anodes that can avoid the above problem [40,41]. Unfortunately, carbon still cannot be adopted successfully in the PEO electrolytes due to the interfacial incompatibility, regardless of its wonderful electrochemical manners in the liquid system. On the other hand, some Li-M-O materials, e.g., spinel $Li_4Ti_5O_{12}$, demonstrate zero-strain effects for Li-insertion, resulting in long cycling life in the solid PEO electrolytes. Relatively low capacity and high Li-insertion potential

of lithium titanates suffers loss of the comparable energy density. In contrast, for the large lithium storage capacity and low operating voltage close to lithium, Li-alloy could be considered as the appropriate candidate. It is believed that the morphology instability, which caused by the volume change of active hosts in association with lithium insertion, severely hinders the development of Li-alloy in both solid and liquid electrolytes. Decreasing particle size and adopting of multi-phase structure is favor for greatly enhancing the cyclability. Some positive results have been obtained, such as Li-Al electrode and interfacial layers of Li-Bi and Li-Pb alloys between lithium metal and solid polymer electrolytes [42,43]. However, the cycling performance of Li-alloy as anode in the solid PEO electrolytes is still poor.

Recently, we have developed a novel lithium ion cell consisting of the composite anode, such as SnSb-$Li_{2.6}Co_{0.4}N$, $SiO_{1.1}$-$Li_{2.6}Co_{0.4}N$, Co_3O_4-$Li_{2.6}Co_{0.2}Cu_{0.2}N$, and the $LiNi_{0.8}Co_{0.2}O_2$ cathode based on the solid PEO-$LiN(CF_3SO_2)_2$ electrolytes [44-48]. Such cells can offer large reversible anode capacity at 450 mAh g^{-1} and high working voltage, as well as an ensured safety without metallic lithium. In this part, the electrochemical performance of several types of novel anodes with the solid-state polymer PEO electrolytes are presented and discussed in detail.

2. Experimental

2.1 Active materials

$LiCo_{0.2}Ni_{0.8}O_2$ (typical particle size is 10 μm) was prepared by the normal solid state reaction. Ultrafine SnSb alloy powder (*ca.* 0.2 μm) was produced by chemical precipitation from aqueous solutions and lithium metal nitrides was synthesized as mentioned above. Nickel powder (99.9%, ca. 0.03 μm), PEO (MW=6 × 10^5), $LiN(CF_3SO_2)_2$, $BaTiO_3$ (typical particle size, ca.0.1μm), PVDF (MW=534000) were commercially purchased. The Co_3O_4 powder (< 2 μm) was obtained by a decomposition reaction of $CoCO_3$ at 800 ^0C in air.

2.2 Polymer electrolyte and cathode film

All the procedure was carries out in the glove box protected by Ar. PEO electrolytes (Li/O ratio: 1/18) were prepared under the casting technique. A given weight of PEO (MW = 6 × 10^5) and $LiN(CF_3SO_2)_2$ was dissolved completely in anhydrous acetonitrile (AN). $BaTiO_3$ was dispersed homogeneously in the solution as filler. The viscous was strongly stirred overnight and cast into a Teflon dish. After AN was slowly and completely evaporated under N_2 flow, the obtained film was further dried at 90 ^0C under vacuum at least 8 h. Cathode films consisting of 52 wt% $LiNi_{0.8}Co_{0.2}O_2$, 10 wt% acetylene black(AB) and 38 wt% PEO-$LiN(CF_3SO_2)_2$ were prepared by the normal casting method similar to PEO film. The thickness of the cathode and PEO film was about 200 μm. The conductivities of the composite polymer electrolyte were observed as high as 1.7x10^{-3} S cm^{-1} at 80 ^0C and 0.82x10^{-3} S cm^{-1} at 65 ^0C.

2.3 Anode preparations

Different preparations were adopted and nominated as (a) dry mixing, (b) wet mixing, (c) hot pressing and (d) casting, respectively. For the dry mixing way, the electrode components were mechanically mixed in an agate mortar. In the case of method (b), the components were homogeneously mixed by the aid of Hexane as a disperser. Polymer binder was added and mixed after Hexane was entirely evicted. Mixtures prepared by (a) and (b) were pressed onto a 280-mesh stainless steel grid, which served as a current collector. Normally, area and thickness of the composite anodes were 0.55 cm^2 and 50-60 μm, correspondingly. Anode prepared by hot pressing was described as follows: PEO powders were carefully sieved and only the smallest particles were passed and used. Before hot pressing, the electrode components were homogeneously mixed and pressed directly onto Cu-foil (20 μm) in a steel mold at a temperature of 70-90℃ and pressure of 10-60 MPa. The press time was 0.5 h-6 h. The thickness of the obtained film was 60-90μm (including Cu-foil). The procedure of method (d) was similar to that of the PEO film preparation. PEO and $LiN(CF_3SO_2)_2$ (Li/O ratio: 1/18) were dissolved in AN solvent entirely. SnSb and conducting Ni powders were added and followed a strong stirring. At last, $Li_{2.6}Co_{0.4}N$ was added at 10 min before the casting. The viscous solution was cast onto a 280-mesh stainless steel grid and further dried at 90 ℃ under vacuum for 2 h.

2.4 Cell assembling and electrochemical measurement

To examine the cycling performance of the composite anode, half-cell was used and metallic lithium was utilized as counter electrode. The full cells were composed of the $LiNi_{0.8}Co_{0.2}O_2$ cathode and the $SnSb-Li_{2.6}Co_{0.4}N$ composite anode. Basically all the three layers, including composite anode, PEO electrolyte and cathode film (or lithium counter electrode), were stacked in coin type cells. A small constant pressure was kept inside cells by the means of the Ni foam as filler. Considering the corrosion instability of Al foil with $LiN(CF_3SO_2)_2$, stainless plate was used as cathode current collector. Thickness ratio of cathode film and current collector is about 1/3. Before assembly, the cathode film was tightly press on the current collector under slightly heat and pressure. Unless stated elsewhere, cycling properties tests were performed at a current density at 0.15 mA cm^{-2} and the working temperature was 65 ℃. The voltage cutoff is 1.4-0.1V vsLi/Li$^+$ and 2.1-3.6V for half cell and full cell respectively. Before electrochemical test, the cells were preheated for 2 hrs at a temperature of 75℃. The discharge capacity was adopted for all figs, corresponding to Li-insertion into the $SnSb-Li_{2.6}Co_{0.4}N$ composite in half-cell and Li-extraction out from the $SnSb-Li_{2.6}Co_{0.4}N$ composite in full cell, respectively.

3. Results and discussion

3.1 Solid-state PEO cells based on SnSb-Li$_{2.6}$Co$_{0.4}$N composite anode

Due to the drastic volume effects in association with Li intercalation into and extraction from SnSb hosts, the anode morphology stability, as well as the interfacial compatibility between the composite anode and the solid PEO electrolytes, dominate the cycling performance of the all solid-state cells. In general, the increased area of electrode is favorable for the electrochemical properties via decreasing the bulk resistance of the cell. However, the non-uniform dispersion of anode components prepared by dry mixing method tends to be aggravation accompanied with the enlarged electrode area. Non-uniform dispersion of lithium salt and nano-Ni conducting powder will cause the relatively low first cycle efficiency and the slightly increased voltage polarization. In addition, ultrafine SnSb particles with non-uniform distribution will form the large aggregation region and easily result in the local volume mismatch during charging and discharging. At last, rapid capacity decline is inevitable. Research reveals that the composite anode prepared by hot pressing and casting way demonstrates severe deterioration compared to dry mixing way.

Based on this, a solution stirring preparation by the aid of a dispersant, e.g., hexane, was introduced to achieve the homogeneous distribution of the electrode components. The cycling stability of the composite electrode prepared by the aid of solvent dispersion is obviously superior to those from other preparations. The observed results suggest that the appropriate anode preparation has an apparent effect upon the electrochemical behavior of the SnSb-Li$_{2.6}$Co$_{0.4}$N composite anode. On the other hand, good electrode performance of the composite electrode requires a combination of suitable polymer binders. Poly(vinylidene fluoride) (PVDF) or poly(vinylidene fluoride)-hexafluoropropylene (PVDF-HFP) as binder in lithium ion batteries demonstrates enough binding ability, high mechanical and chemical stability even at elevated temperature. The electrochemical stable window of fluorinated polymers is as wide as 0 to 5 V vs. Li/Li$^+$. Moreover, these polymers are easer to be dispersed and can improve the adhesion between the active material and current collector. The mechanical strength of the composite electrode can be greatly reinforced by the use of PVDF as framework due to its strong binder ability for retraining the morphological instability in the Li-alloy processing, indicating that the function of fluorinated polymer and PEO-LiX as binder is mainly corresponding to sustain morphological stability and supply ionic channels within composite electrode respectively. Ionic conductivity predominates in the amorphous rather than crystalline regions of PEO electrolytes. The local relaxation and segmental motion of the polymer chains appears to be a requirement for lithium ion transport. The effect of operating temperature on mechanical strength and ionic movement of polymer electrolytes is contradictory. Therefore, it is reasonable that the SnSb-Li$_{2.6}$Co$_{0.4}$N electrode performance exhibits a strong dependence on the environment temperature, as shown in Fig.31, in which the coulombic efficiency at the first cycle apparently decreases with increasing the temperature. It is noted that capacity lessen in the lithium extraction process is mainly attributed to shortness of voltage plateau near 1.1 V, which is related to Li$_{2.6}$Co$_{0.4}$N active material. This indicates that the Li$_{2.6}$Co$_{0.4}$N may lose some activity at high temperature in PEO-LiX system and it is the main reason

for the reduced charge recovery in the subsequent cycles.

The deterioration of the mechanical performance of polymer PEO electrolyte at high temperature also takes part consequence. The temperature as a function upon the capacity-cycling behavior was shown in the inset in Fig.31. Below the melting point of PEO (ca. 65°C), the polymer electrolyte delivers enough mechanical strength and can hold good interfacial morphology stability between electrode and electrolyte. In addition, the relative rigidity of PEO-LiX at low temperature within composite electrode is favorable for restraining the volume expands of SnSb hosts for Li-insertion. However, low operating temperature corresponds to a poor interface contact and slow Li-transfer in both composite electrode and polymer electrolyte layers, resulting in a small capacity and unsteady cyclability. The capacity increases remarkably near PEO melting point due to adhesive interface contact and high ionic conductivity. It seems that such a cell system works poorly if the operating temperature continually grows over 75°C. At elevated temperature, sticky or even viscous property of the PEO-LiX in combination with the drastic volume effect of active SnSb particles will bring about a server mechanical instability of the electrode. The morphological change could be aggravated and hardly be recovered for the PEO-containing system above 75°C under strict pressure inside cells. The appropriate operating temperature for the SnSb-$Li_{2.6}Co_{0.4}N$ composite electrode is between 65 and 75°C. However such electrodes demonstrate a quite stable interfacial contact with polymer electrolytes during storage over a wide operating temperature. The interface resistance between composite electrode and solid electrolytes is acceptable even at 60 °C, as shown in the inset (1) in Fig.32, because the cell was preheated at a temperature 10°C higher than operating one before test. With increasing temperature, the impedance is greatly reduced, suggesting a significant improvement in the interfacial contact, as shown in the inset (2) in Fig.33. Dispersing $BaTiO_3$ in polymer binders may greatly reinforce the mechanical strength of PEO-LiX within composite electrode and, as a consequence, improves the morphology and cycling stability of whole electrode during charging and discharging. The typical charge and discharge profiles of the solid PEO Li-ion cell based on SnSb-$Li_{2.6}Co_{0.4}N$ composite anode and the $LiNi_{0.8}Co_{0.2}O_2$ cathode at 65°C are given in Fig.33. The $LiNi_{0.8}Co_{0.2}O_2$ cathode can deliver a reversible capacity about 140 mAh g^{-1} at appropriate working voltage scales in PEO-$LiN(CF_3SO_2)_2$-$BaTiO_3$ system, about one forth of that of the composite anodes. For full utilization of lithium storage capacity of composite anode, the weight of cathode has to be much over that of anode (4-5 times). A little increase of voltage plat from the first cycle to the following ones can be observed and it is mainly linked to the phase transfer of $Li_{2.6}Co_{0.4}N$ from crystal to amorphous state. It is attractive that a high coulombic efficiency over 94 % and a large reversible anode capacity about 500 mAh g^{-1} at the first cycle can be obtained in this system. Moreover, the capacity remains stable of above 400 mAh g^{-1} after 30 cycles under the limited lithium insertion. The capacity fade during cycling could be greatly prevented via the suitable charge-discharge control and the proper cell structure. A further improvement for cycling performance of the cells is still on the progression.

3.2 Electrochemical behavior of $SiO_{1.1}$-$Li_{2.6}Co_{0.4}N$ anode with the PEO electrolytes

The charge and discharge profiles of the $SiO_{1.1}$-$Li_{2.6}Co_{0.4}N$ composite electrode with the PEO electrolytes at different cycles are shown in the inset in Fig.34. The insertion capacity was increased to about 550 mAh g^{-1} at the second cycle, vs. 420 mAh g^{-1} at the first cycle. It is probably attributed to a reduced polarization caused by the improved electrochemical kinetics at the electrode interface compatibility. The voltage trends of the composite reflect mixing potential characteristics of $SiO_{1.1}$ and $Li_{2.6}Co_{0.4}N$ active materials. In fact, the capacity above 0.8 V from $Li_{2.6}Co_{0.4}N$ plays an important role for the compensation for the irreversible capacity. As a result, a high first cycle efficiency of ca.100% was obtained. The electrode compositions have an apparent influence upon the electrochemical behavior of the electrode, similar to that of the $SnSb$-$Li_{2.6}Co_{0.4}N$ electrode. Fig.34 shows the capacity change as a function upon the cycle number of the $SiO_{1.1}$-$Li_{2.6}Co_{0.4}N$ composite electrodes at various environment temperatures. The reversible capacity in the cycling beginning was improved with increasing the temperature due to the adhesive interface contact and high ionic conductivity. However, high temperature fast the capacity fading. It indicates that an aggravated decay in the mechanical strength of the PEO electrolytes can hardly endure the morphology instability arising from silicon. By contrast, PEO electrolyte at low temperature possesses a high mechanical stability with a low ionic conductivity that leads to a small capacity with good capacity retention. It was further found that dispersing sub-micro ceramic $BaTiO_3$ within the electrode is in favor for the cycling behavior of the composite electrode. Ceramic fillers, such as $BaTiO_3$ and Al_2O_3, can improve the mechanical performance of the flexible PEO electrolyte and stabilize the interfacial properties at elevated temperature. Furthermore, it can reduce the crystallizing tendency of the polymer electrolyte; thereby it enhances the ionic conductivity. With temperature increasing, the solid PEO-$LiN(CF_3SO_2)_2$ composite electrolyte turns into be serious sticky and fluid. The function of $BaTiO_3$ is to enhance the mechanical strength of the electrolyte components within the composite electrode that could maintain the electrode integrity. Research reveals that the suitable current density for this composite electrode in the solid PEO electrolytes is between 0.1 and 0.5 mA cm^{-2} after tradeoff capacity and capacity retention.

3.3 Electrochemical behavior and thermal performance of the Co_3O_4-$Li_{2.6}Co_{0.2}Cu_{0.2}N$

The Co_3O_4-$Li_{2.6}Co_{0.2}Cu_{0.2}N$ composite demonstrate reasonable interfacial compatibility with PEO electrolytes and thus good electrochemical behavior. The capacity changes, as a function of cycling, for different anodes with the solid PEO-based polymer electrolytes are shown in Fig. 34. The reversible capacity of graphite was below 200 mAh g^{-1} and the charge and discharge efficiency in the first several cycles was extremely low. Moreover, its capacity retention suffered from an obvious fading during cycling. The $SnSb$-$Li_{2.6}Co_{0.4}N$ anode had a large capacity of over 600 mAh g^{-1} and high coulombic efficiency of ca. 100 % in the first cycle. However, a gradual deterioration in the cycling

performance was always observed due to the volume effects of alloys. The capacity fade was significantly suppressed for the $Li_{2.6-x}Co_{0.2}Cu_{0.2}N-Co_3O_4$ anode and estimated to be only about 0.37%/cycle during cycling. The charge and discharge profiles of the $Li_{2.6-x}Co_{0.2}Cu_{0.2}N-Co_3O_4$ anode at 65 ℃ as shown in the inset in Fig.34 indicate that the charge-discharge efficiency was almost 100% and lithium can be intercalated and extracted with a high reversibility. In general, the safety of small size lithium-ion cells under normal use is well established. In contrast, the safety of the large size lithium-ion batteries is still questionable, especially in cases of abusive use. Safety of lithium ion batteries is mainly related to the thermal reactivity of the electrode components. We found that specific reaction heats, which indicates the thermal stability and safety of the battery system, for the $Li_{2.6}Co_{0.2}Cu_{0.2}N-Co_3O_4$ anode charged up to 0.01 V vs. Li/Li$^+$ was estimated to be 1.1 J mAh^{-1}. Those for $Li_{2.6}Co_{0.2}N-SnSb$ anode was 2.75 J mAh^{-1}. The specific reaction heat for lithium metal and PEO electrolyte (1:1 weight ratio) is 1.24 J mAh^{-1}. However, in practice, for the case of a lithium metal anode, an excess amount of lithium metal, at least four times compared to the cathode capacity, should be used because of the dendrite formation on the anode. Therefore, the reaction heat of lithium metal with PEO electrolytes was estimated to reach 4.96 J mAh^{-1} or higher. Therefore, the $Li_{2.6}Co_{0.2}Cu_{0.2}N-Co_3O_4$ anode shows the lowest reaction heat, indicating that the novel anode has potential applications in the large size rechargeable lithium-ion batteries for EV & HEV.

Conclusions

Anode material, which possesses large capacity density, high first cycle efficiency and low reaction heating with the PEO electrolytes, is the key for developing lithium polymer rechargeable batteries that proposed for extremely demanding applications such as electric vehicles (EV) and hybrid electric vehicles (HEV). By this motivation, we have developed series novel composite anode which show good electrochemical behavior with the PEO electrolytes. We are at present investigating the performance of the all solid-state PEO cells with these proposed novel anodes and some typical high potential cathodes

References

[1] J.-M. Tarascon and M. Armand, Nature 414,359-367 (2001)

[2] S. Eckfeld, J.E. Manders, M.W. Stevenson, J. Power Sources 5105 (2003) 1-8

[3] S. Levaesseur,M.Menetrier,C. Delmas, J. Electrochem. Soc. 149 (2002) A1533.

[4] A.K. Padhi, K.S. Nanjundaswamy, J.B. Goodenough, J. Electrochem.Soc. 144 (1997) 1188

[5] K. Sato, M. Noguchi, A. Demachi, N. Oki, M. Endo, Science 264 (1994) 556

[6] M. Winter, J.O. Besenhard, Electrochimica Acta 45, (2003) 31

[7] M. Nishijima, T. Kagohashi, N. Imanishi, Y. Takeda, O. Yamamoto and S. Kondo, Solid State

Ionics, 83 (1996) 107

[8] P. Poizot, S. Laruelle, S. Grugeon, L. Dupont, J-M. Tarascon, Nature 407 (2000) 496

[9] Y. Idota, T. Kubota, A. Matsufuji, Y. Maekawa, T. Miyasaka, Science 276 (1997) 1395

[10] J.-M. Tarascon and M. Armand, Nature 414 (2001) 359-367

[11] M. Winter, J.O. Besenhard, Electrochimica Acta 45 (2003) 31

[13]C.J. Wen and R.A. Huggins. J. Solid State Chem. **37** (1976) 271

[14]K. Amezawa, N. Yamamoto, Y. Tomii and Y. Ito. J. Electrochem. Soc. 145 (1998) 1986

[15]H. Li, X.J. Huang, L.Q. Chen, G.W. Zhou, Z. Zhang, D.P. Yu, Y.J. Mo, N. Pei, Solid State Ionics, 135 (2000) 181

[16] P. Limthongkul, Y. Jang, N.J. Dudney, Y.M. Chiang, Acta Materialia, 51 (2003) 1103.

[17]A. Netz, R.A. Huggins, W. Weppner, J. Power Sources, 5271, 1 (2003); Il-S. Kim, P.N. Kumta, G.E. Blomgren, Electrochem. Solid-State Lett., 3, 493 (2000); H.Y. Lee, S.M. Lee, J. Power Sources, 112, 649 (2002);.Il-S. Kim, G.E. Blomgren, P.N. Kumta, Electrochem. Solid-State Lett., 6, A157 (2003); H. Dong, X. P. Ai and H. X. Yang, Electrochemistry Communications, 5, 952 (2003); Il-S. Kim, G.E. Blomgren, P.N. Kumta, J. Power Sources, 130, 275 (2004); N. Dimov, S. Kugino and M. Yoshio, J. Power Sources, 136, 108 (2004); H. Dong, R.X. Feng, X.P. Ai, Y.L. Cao and H.X. Yang, Electrochimica Acta, 49, 5217 (2004).

[18]Y. Liu, et al, Mie university, 3A11; H. Uono, et al, Mitsubishi chemical group, 1D11; M. Yamada, et al, Hitachi Maxell, Ltd., 1D 12; T. Morita, et al, Toshiba, 1D13; The 44th Battery Symposium in Japan, 2003, Sakai.

[19] Z.S. Wen, J. Yang, B.F. Wang, K. Wang, Y. Liu, Electrochemistry Communications 5, 165 (2003); Y. Liu, K. Hanai, J. Yang, N. Imanishi, A. Hirano, Y. Takeda, Solid State Ionics, 168, 61 (2004); J. Yang, B.F. Wang, K. Wang, Y. Liu, J.Y. Xie, Z.S. Wen, Electrochem. Solid-State Lett., 6, A154 (2003); Y. Liu, K. Hanai, J. Yang, N. Imanishi, A. Hirano, Y. Takeda, Electrochem. Solid-State Lett., 7, A369 (2004); Y. Liu, K. Hanai, T. Matsumura, N. Imanishi, A. Hirano and Y. Takeda, Electrochem. Solid-State Lett., 7, A492 (2004); Il-Seok Kim and Prashant N. Kumta, J. Power Sources, 136, 145 (2004); G.X. Wang, J.H. Ahn, J. Yao, S. Bewlay and H.K. Liu, Electrochemistry Communications, 6, 689 (2004); X.W. Zhang, P.K. Patil, C. Wang, A.J. Appleby, F.E. Little and D.L. Cocke, J. Power Sources, J. Power Sources, 125, 206 (2004).

[20] N. Dimov, K. Fukuda, T. Umeno, S. Kugino, M. Yoshio, J. Power Sources 5030, 1 (2002); X.Q. Yang, J. McBreen, W.S. Yoon, M. Yoshio, H.Y. Wang, K.J. Fukuda, T. Umeno, Electrochemistry Communications 4, 893 (2002); N. Dimov, S. Kugino, M. Yoshio, Electrochimica Acta 48, 1579 (2003).

[21]T. Yamamoto, et al, Matsushita Battery Industrial Co., Ltd., 2D-06; Y. Ono, et al, Mie University, 2D-13. The 46th Battery Symposium in Japan, 2005, Nagoya.

[22] M. Nishijima, T. Kagohashi, N. Imanishi, Y. Takeda, O. Yamamoto, J. Power Sources, 68 (1996) 510

[23] S. Suzuki, T. Shodi and J. Yamaki, J. Phys. Chem. Solids, 59 (1998) 331

[24] T. Shodi, S. Okada, S. Tobishima and J. Yamaki, J. Power Sources 68 (1997) 515

[25] T. Shodi, Y. Sakurai and T. Suzuki, Solid State Ionics 122 (1999) 85

[26] T. Y. Kim, M. G. Kim, J. M. Lee, T. Kang and H. J. Sohn, Electrochemical and Solid-State Letters, 5 (2002) A103

[27] Y. Takeda, M. Nishijima, M. Yamahata, K. Takeda, N. Imanishi and O. Yamamoto, Solid State Ionics, 130 (2000) 61

[28] J. Yang, Y. Takeda, N. Imanishi and O. Yamamoto, J. Electrochem. Soc., 147 (2000) 1671

[29] J. Yang, Y. Takeda, N. Imanishi and O. Yamamoto, Electrochimica Acta, 46 (2001) 2659

[30] Y. M. Kang, S. C. Park, Y. S. Kang, P. S. Lee and J. Y. Lee, Solid State Ionics 156 (2003) 263

[31] Y. Liu, K. Horikawa, M.Fujiyosi, N. Imanishi, A. Hirano and Y. Takeda, J. Electrochem. Soc., 151 (2004) A1450

[32] Y. Liu, T. Matsumura, N. Imanishi, T. Ichikawa, A. Hirano, Y. Takeda, Electrochemistry Communications 6 (2004) 632

[33] Y. Liu, K. Horikawa, M. Fujiyosi, N. Imanishi, A. Hirano and Y. Takeda, Electrochimica Acta 49 (2004) 3487

[34] Y. Liu, K. Horikawa, M. Fujiyoshi, T. Matsumura, N. Imanishi and Y. Takeda, Solid State Ionics, 172 (2004) 69

[35] Y. Liu, N. Imanishi, A. Hirano, T. Matsumara and Y. Takeda, Electrochem. Solid-State Lett., in submission

[36] Y. Liu, K. Hanai, K. Horikawa, N. Imanishi, A. Hirano and Y. Takeda, Materials Chemistry & Physics, in press

[37] Y.Aihara, M.Kodama, K.Nakahara, H.Okise, K. Murata, J.Power Sources. Vol.65 pp.143-148 (1997).

[38] F. Croce, B. Scrosati, J. Power Sources.Vol.43-45, pp.9-12 (1993).

[39] I.M. Ismail, U. Kadiroglu, N. D. Gray, J. R. Owen, in: Electrochemical Society Meeting Abtracts, San Antonio, TX, Oct. 6-12 Vol. 96-2,1999, Abstract 63.

[40] D. Fauteux and R. Koksbang, J. Appl. Electrochem. Vol.23, pp.1-6 (1993).

[41] J. O. Besenhard, J. Yang and M. Winter, J. Power Sources 68 (1997) 87

[42] A. Belanger, M. Robitaille, US patent 4652506, 1989.

[43] M. Hiratani, K. Miyauchi, T. Kudo, in: Int.Conf Solid State Inoics, Garmish 28-30 (1988) 1431

[44] J. Yang, Y. Takeda, Q. Li, N. Imanishi, O. Yamamoto, J. Power Sources 90 (2000) 64

[45] J. Yang, Y. Takeda, Q. Li, N. Imanishi, O. Yamamoto, J. Power Sources 97-98 (2001) 779

[46] J. Yang, M. Wachtler, M. Winter, J. O. Besenhard, Electrochem. Solid State Lett. 2 (1999) 161.

[47] Y. Liu, J. Yang, N. Imanishi, A. Hirano, Y. Takeda, and O. Yamamoto, J. Ceramic Society of Japan 112 (2004) s638.

[48] Y. Liu, J. Yang, N. Imanishi, A. Hirano, Y. Takeda and O. Yamamoto, J. Power Sources, in press
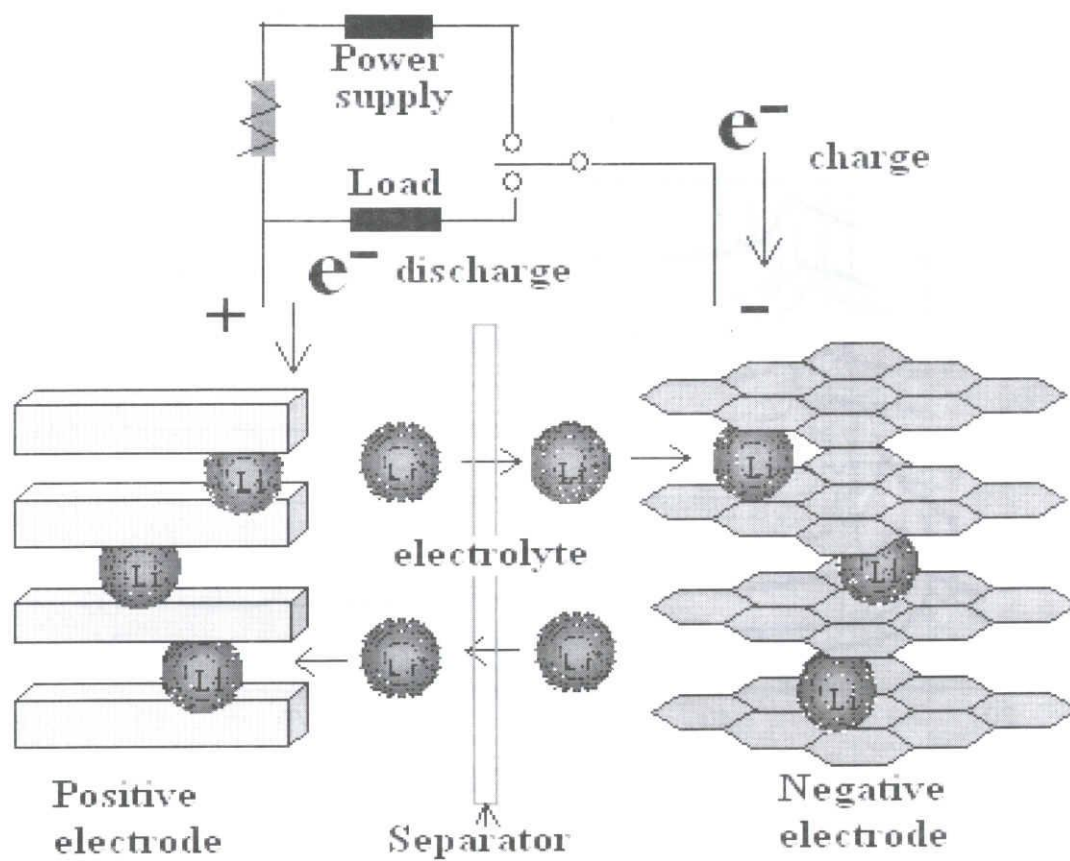
Fig.1. Principle of the lithium ion cell.
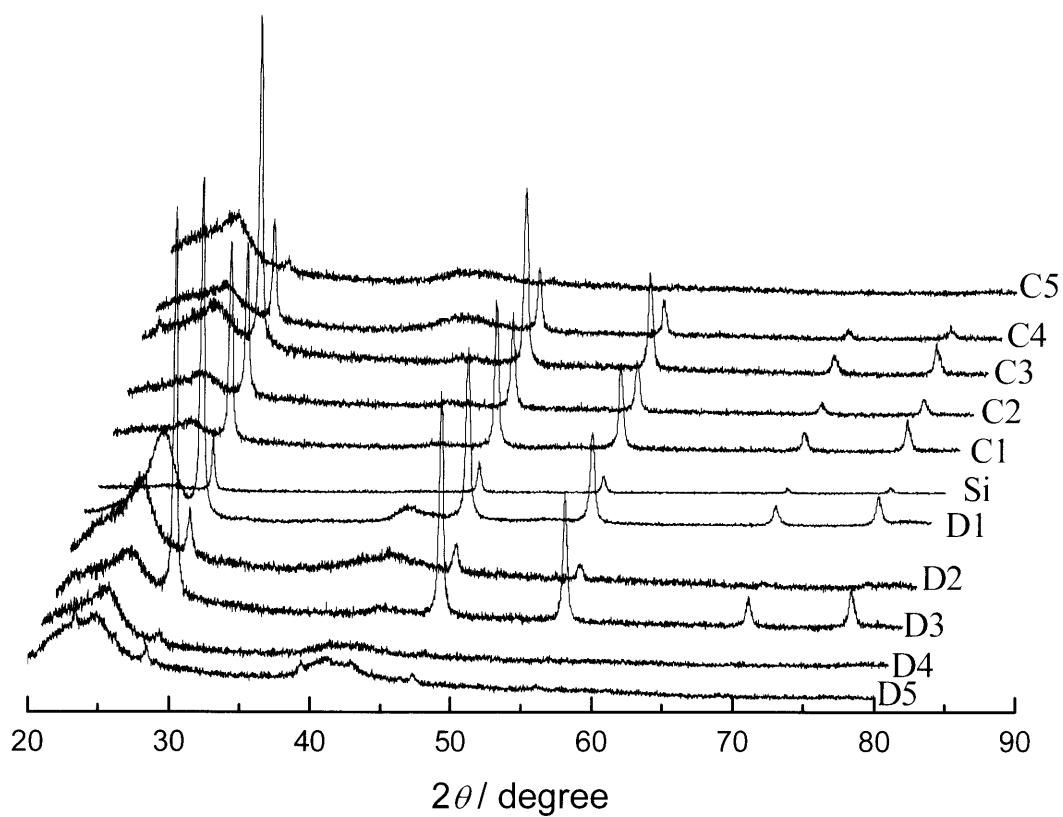
Fig.2. XRD patterns of starting Si (< 1μm) upon different charge and discharge depth, while D1-D5 relates to Li-insertion into Si until 200, 100, 75, 50, 20 mV vs. Li/Li$^+$, and further keep such a potential until current density to 0; C1-C5 relates to Li-extraction from Si at D1-D5 stages, respectively, until to 1.5 V vs. Li/Li$^+$.
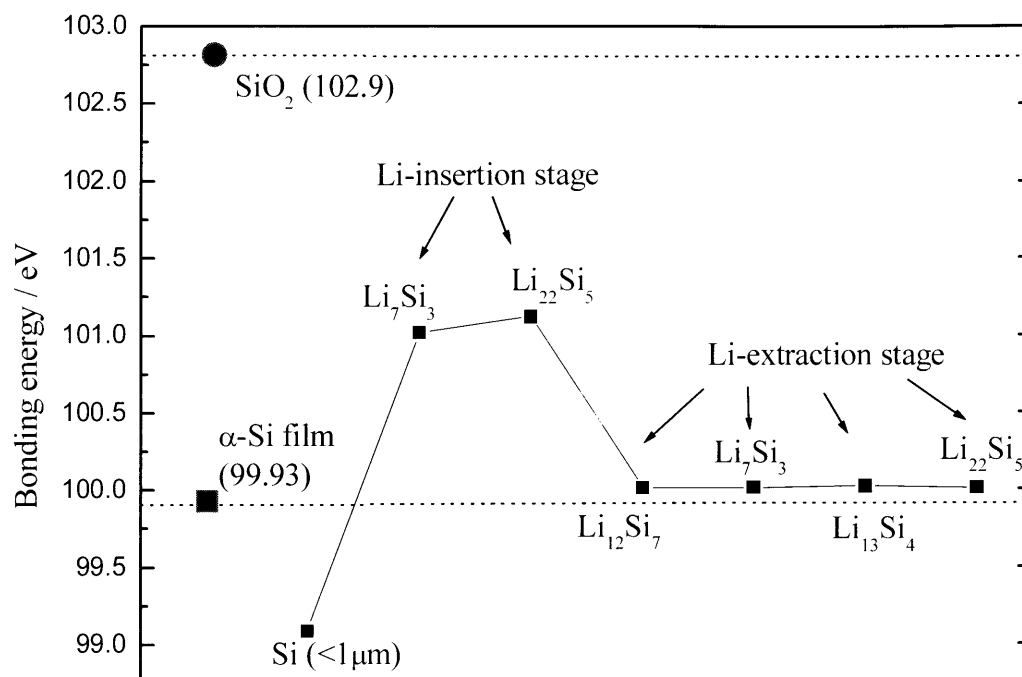
Fig.3. Chemical bonding energy of Si2P (3/2) upon different Li-intercalation and extraction depth based on XPS measurements.
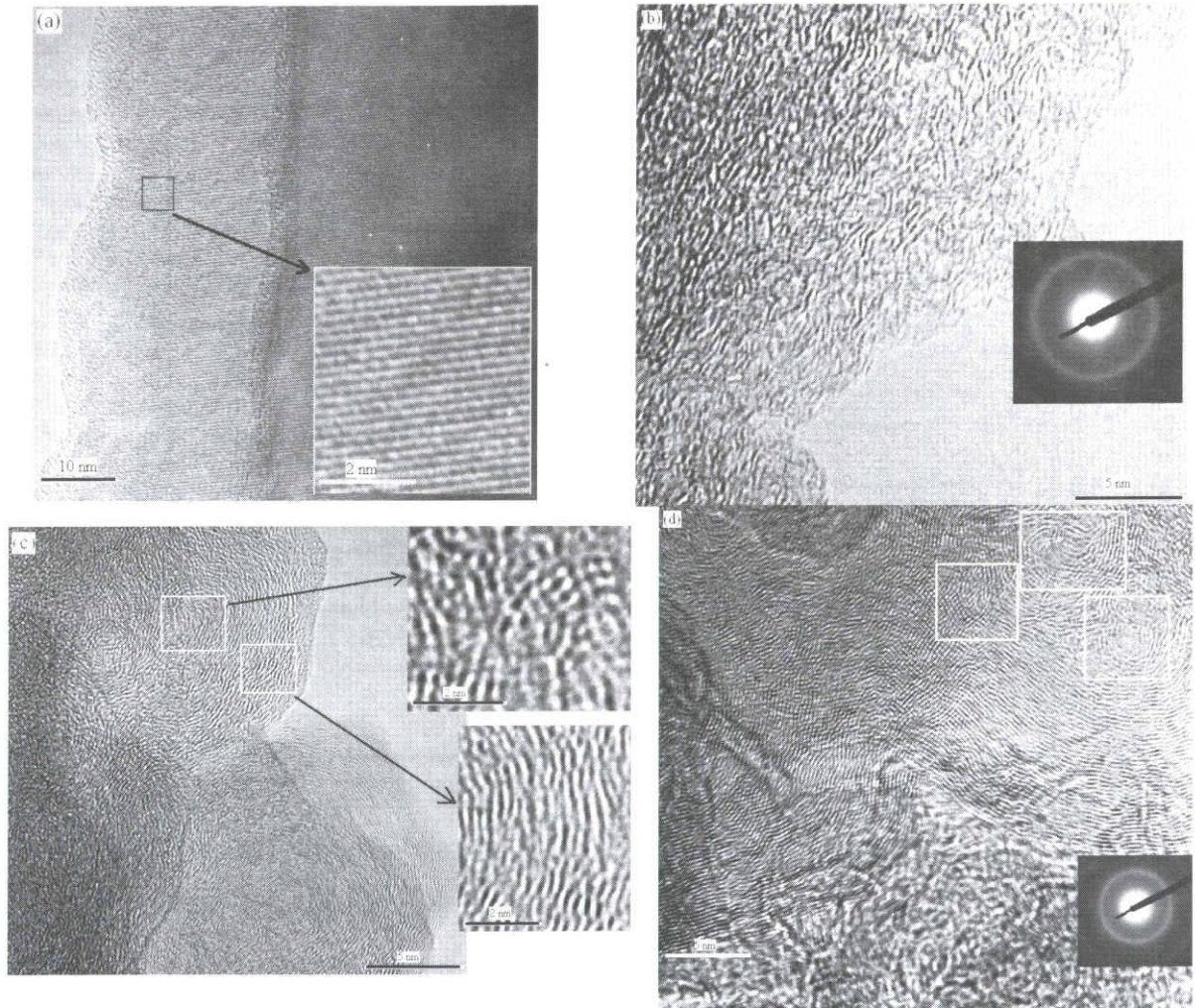
Fig.4 a-d: HRTEM images of a) starting Si (<1 μm), b) Li-insertion into Si (60 nm) until at $Li_{22}Si_5$ stage; c) Li-extraction from Si (60 nm, at $Li_{22}Si_5$ stage), and d) Li-extraction from Si (< 1μm, at $Li_{22}Si_5$ stage).
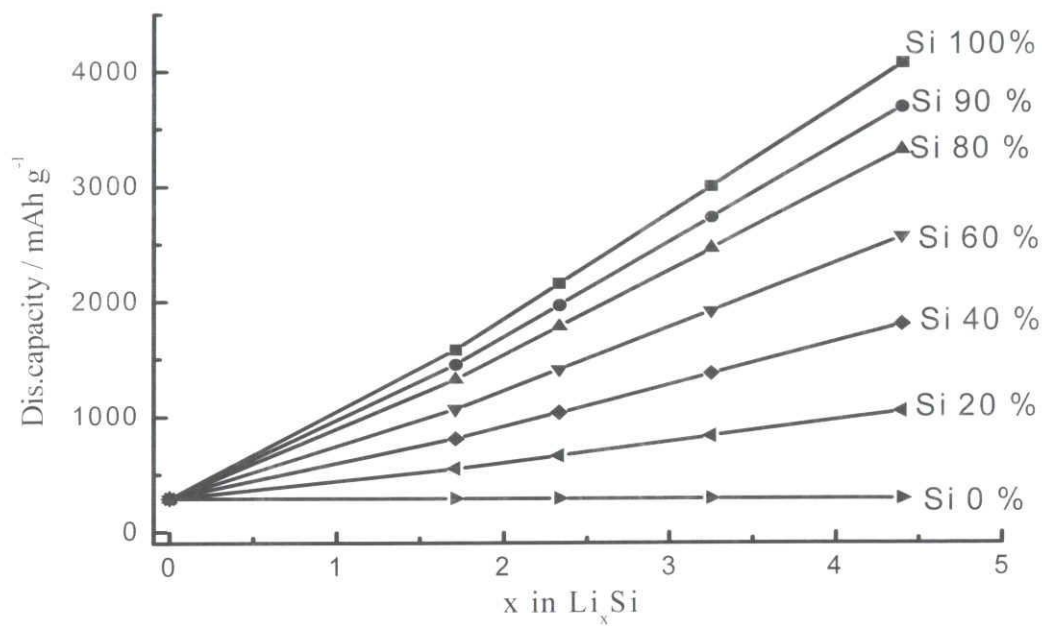
Fig.5. Function of the Si-contents and Li-reaction depths upon the capacity of the Si/C composites
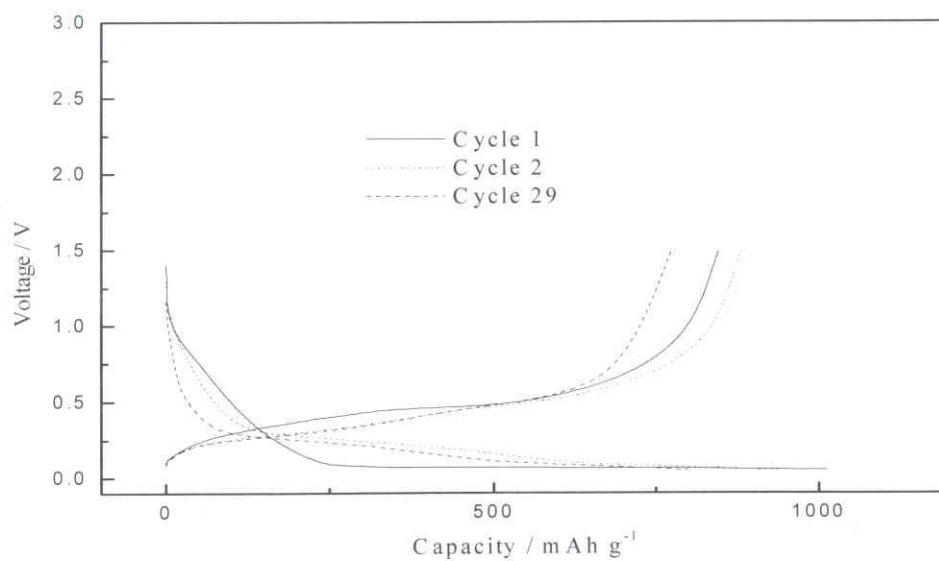
Fig.6. Charge and discharge profiles of the resulting Si/C composite, 0.02-1.5 V vs. Li/Li$^+$.
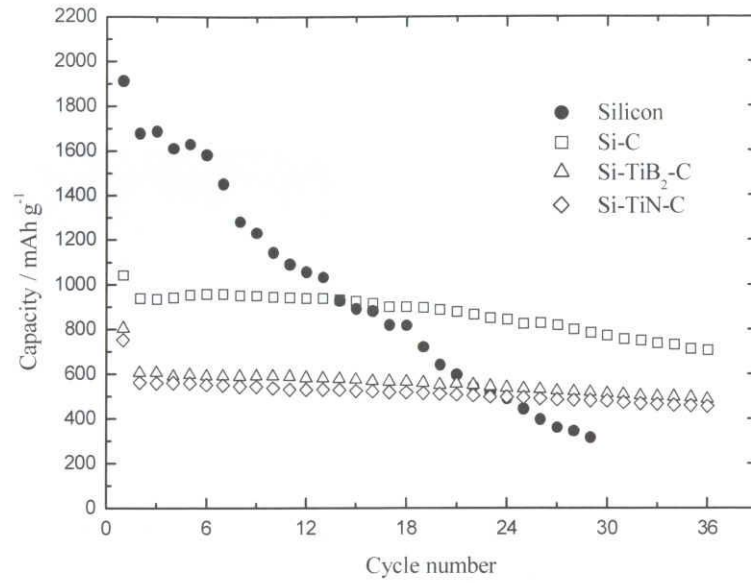
Fig.7. Cycling performance of the resulting Si based composites, 0.02-1.5 V vs. Li/Li$^+$.
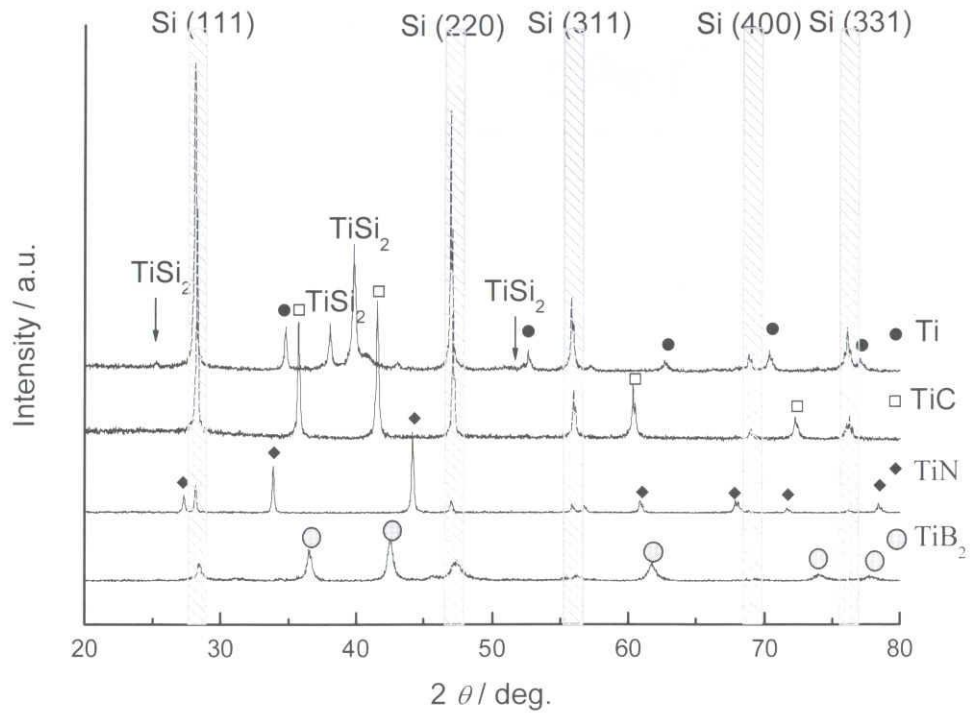
Fig.8. XRD patterns of the ball-milled Si-M (M=Ti, TiN,TiB$_2$, and TiC) under Ar of certain time.
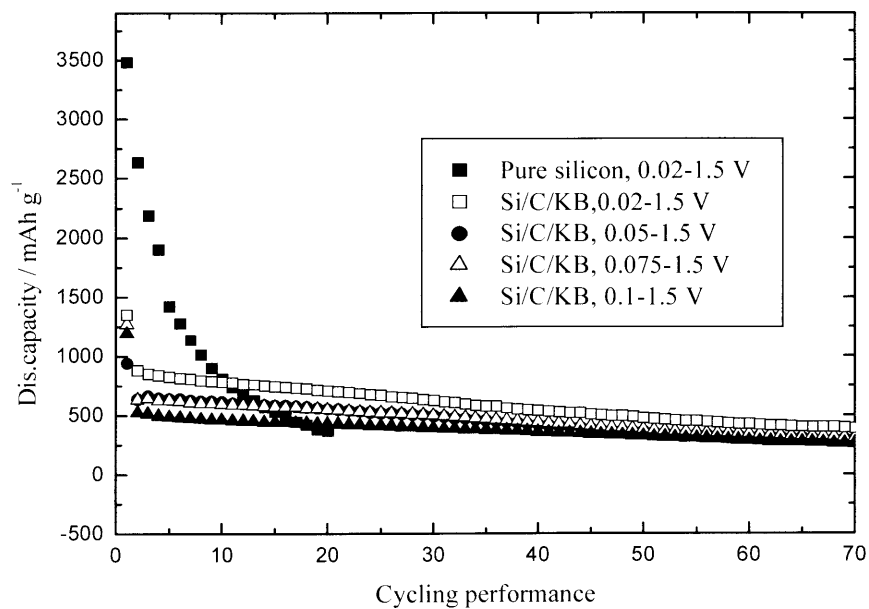
Fig.9. Cycling performance of the Si/C composites based on nano-Si (60 nm) and carbonaceous fillers.
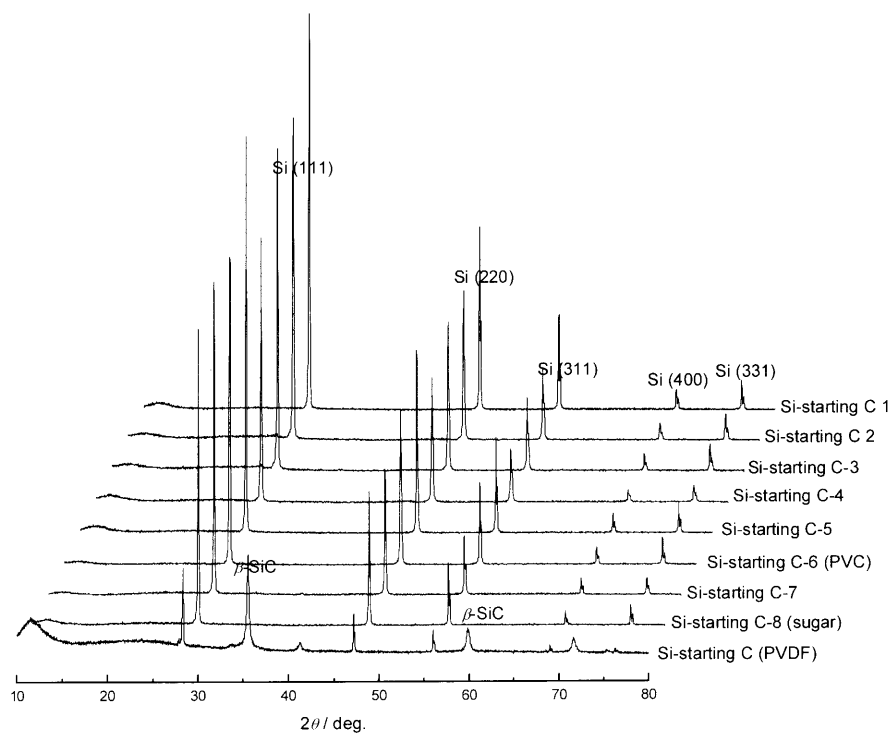
Fig.10. XRD patterns of the pyrolyzed Si/C composites based on different carbonaceous precursors
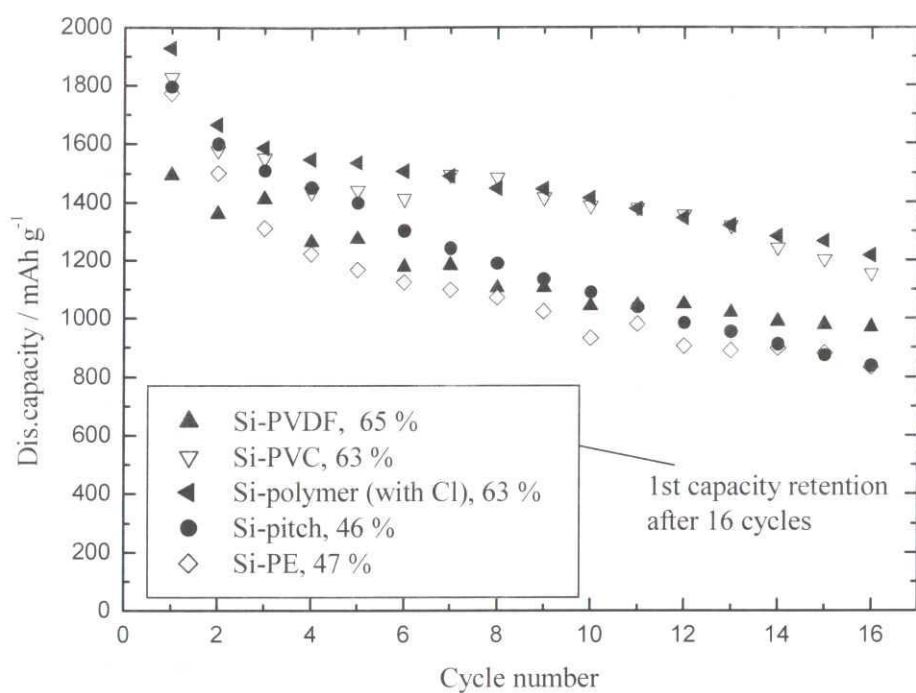
Fig.11. Cycling performance of the pyrolyzed Si/C composites based on different carbonaceous precursors.
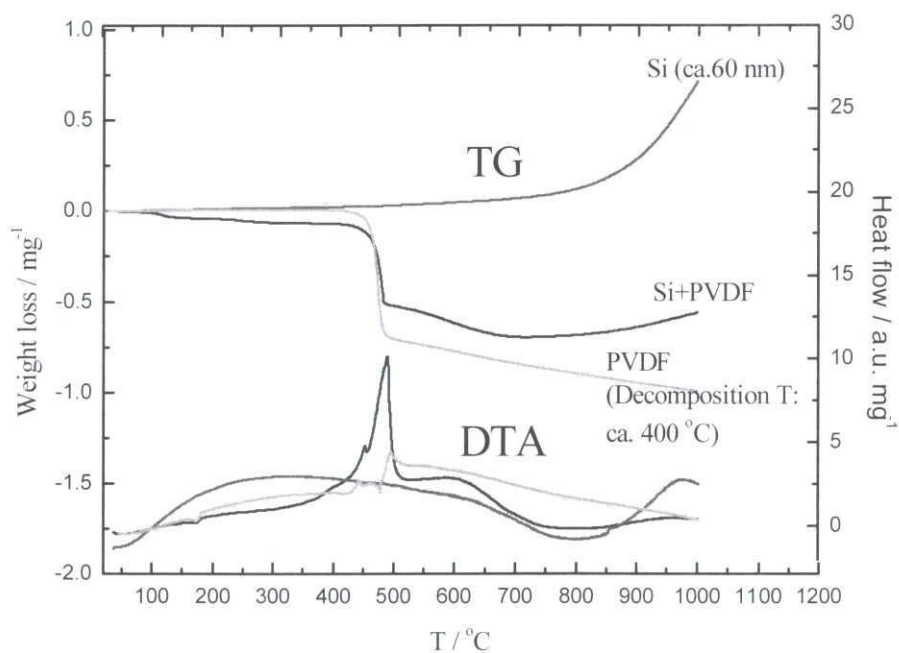
Fig.12. TG-DTA curves of the Si, Si-PVDF, and PVDF upon heating to 1000 °C in N_2, heating rate of 5°C/min.
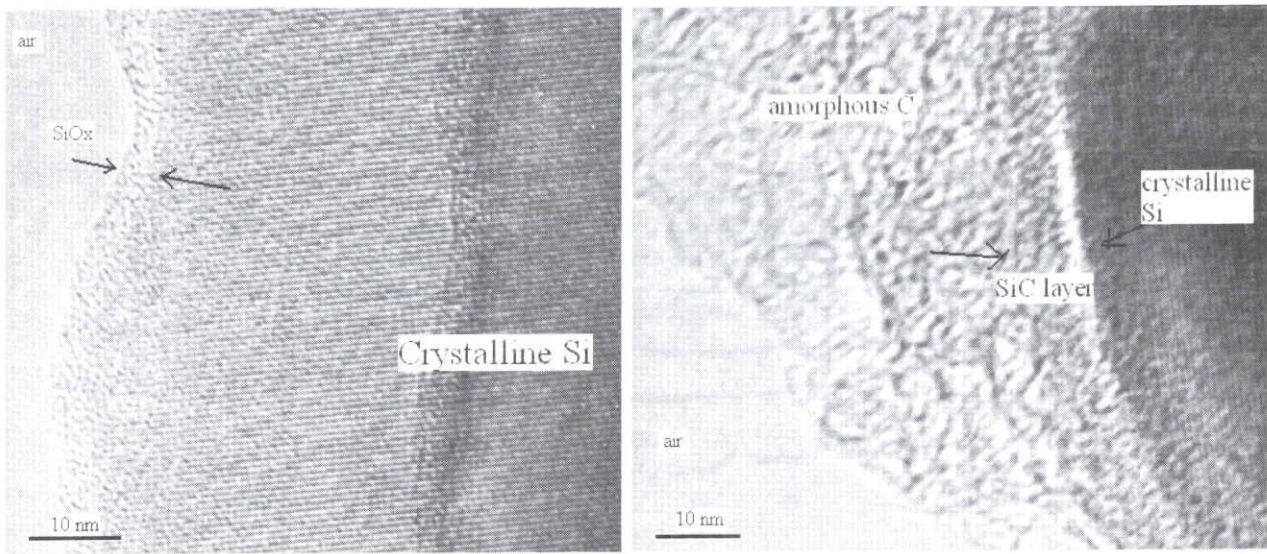
Fig.13. HRTEM images of the pure Si and pyrolyzed Si/C composite.
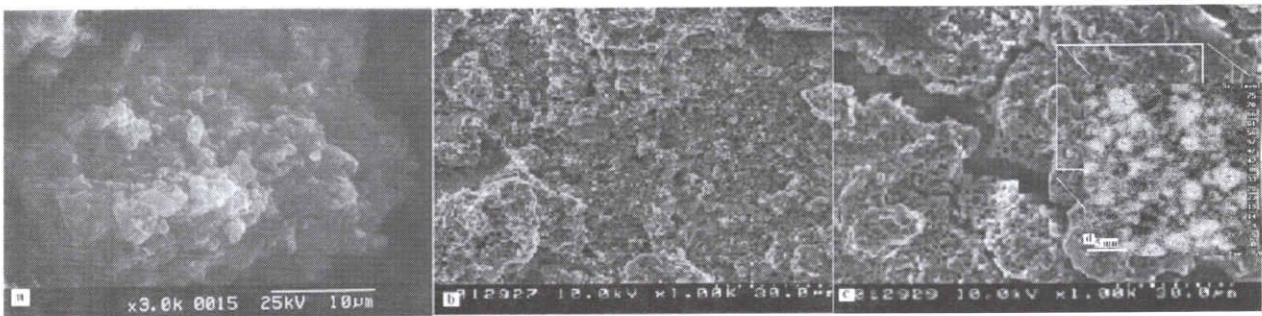
Fig.14. Cross-sectional SEM photographs of the Si/C based composites at: a) before cycles, b) after 30 cycles, and c) after 200 cycles and EPMA image of elemental-Si distribution at the selected area from c;
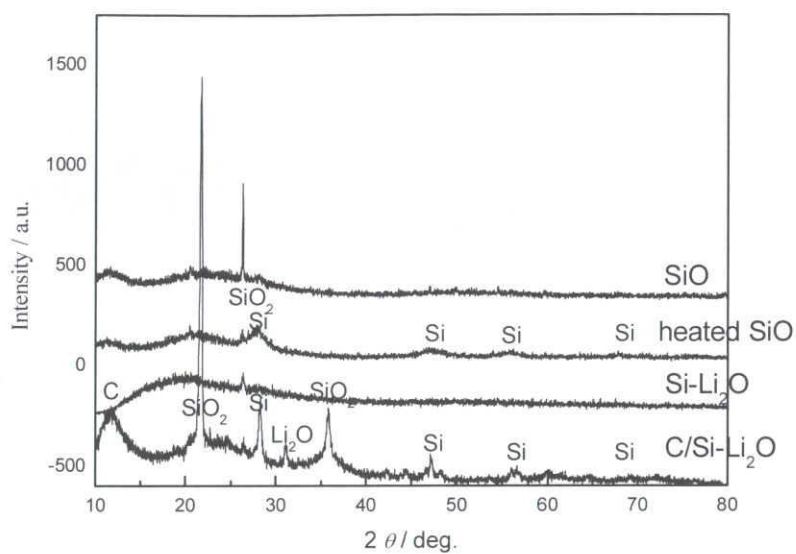
Fig.15. XRD patterns of the resulting products based on SiO upon different treatment
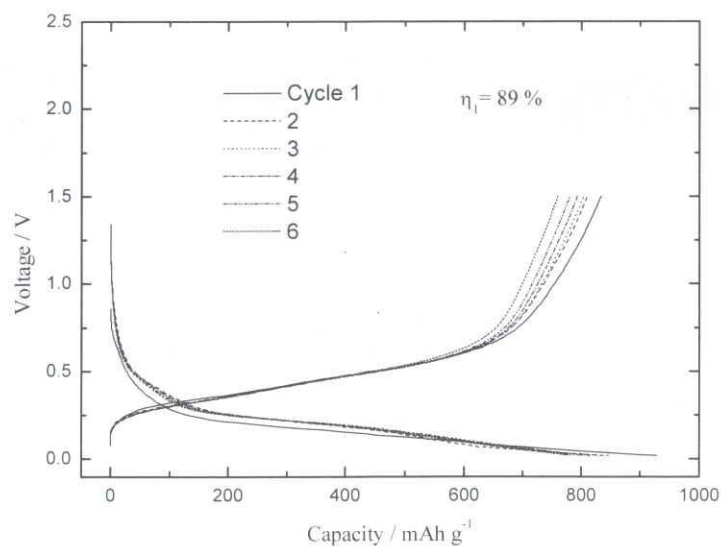
Fig.16. Charge and discharge profiles of the resulting Si-Li$_2$O composite, 0.02 -1.5 V vs. Li/Li$^+$.
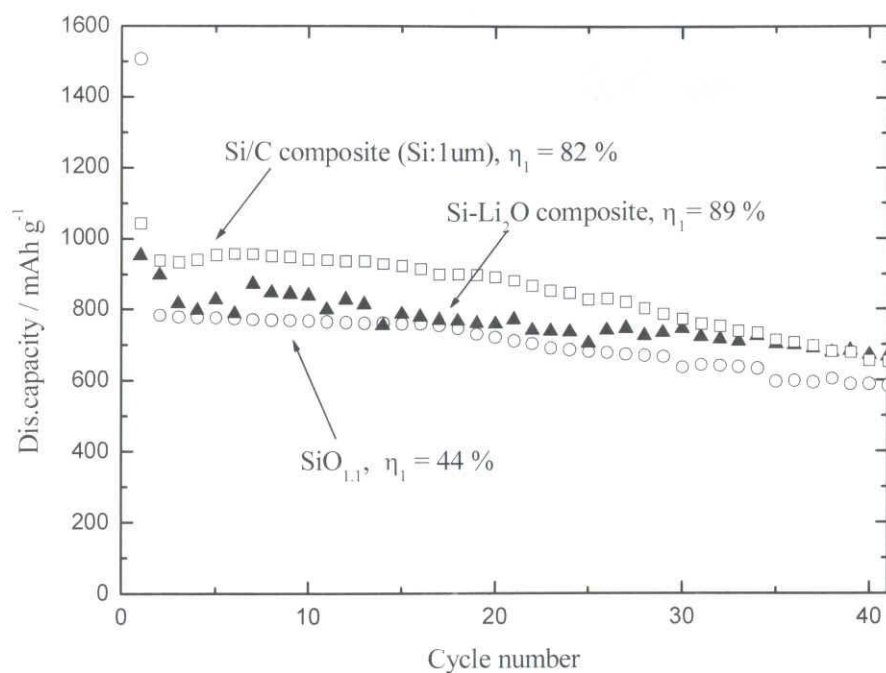
Fig.17. Cycling performance of different Si based electrodes.
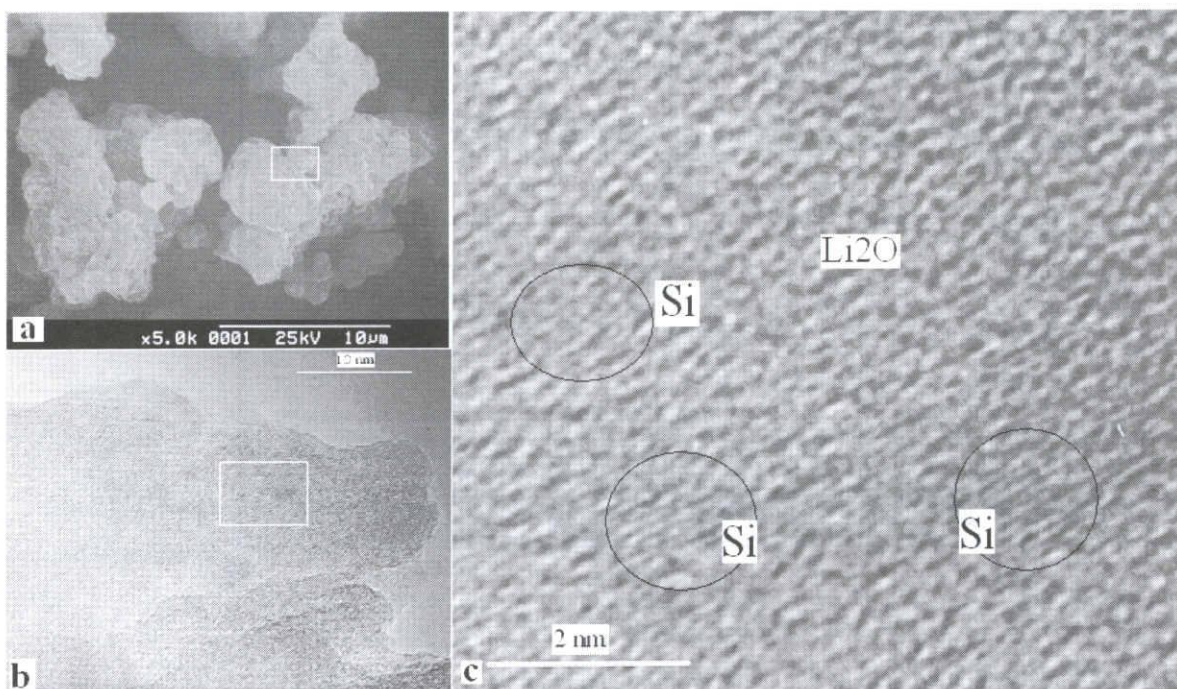
Fig.18 a) SEM image of the resulting Si-Li₂O composite; b) TEM image of the selected area from a; and c) HRTEM image of the selected area from b.
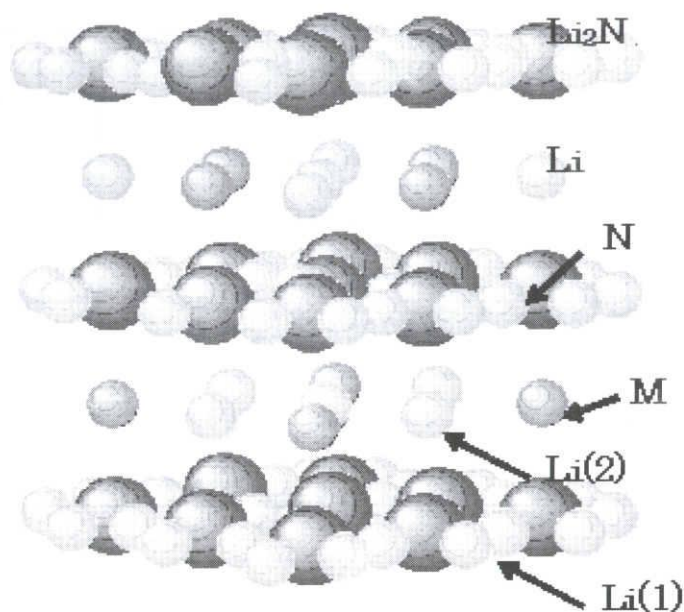
Fig.19. Structure model of the $Li_{2.6}Co_{0.4}N$.
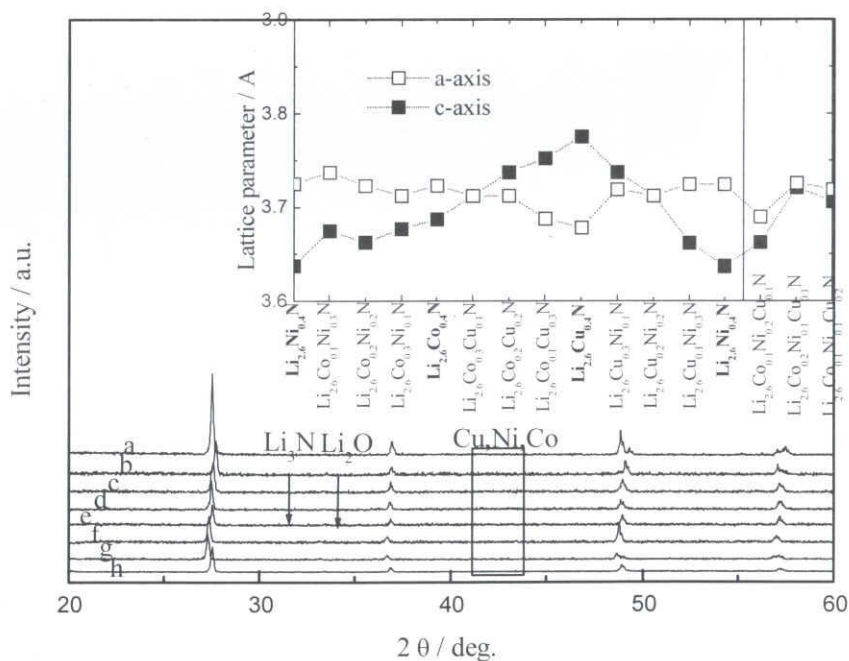
Fig.20. XRD patterns of the hexagonal lithium metal nitrides: a) $Li_{2.6}Co_{0.4}N$; b) $Li_{2.6}Co_{0.2}Cu_{0.2}N$; c) $Li_{2.6}Co_{0.2}Ni_{0.2}N$; d) $Li_{2.6}Cu_{0.2}Ni_{0.2}N$; e) $Li_{2.6}Co_{0.25}Cu_{0.15}N$; f) $Li_{2.6}Co_{0.2}Cu_{0.1}Ni_{0.1}N$; g) $Li_{2.6}Co_{0.25}Cu_{0.1}Ni_{0.05}N$; h)$Li_{2.6}Co_{0.2}Cu_{0.15}Fe_{0.05}N$. The inset figure is Lattice parameters of the lithium metal nitrides.
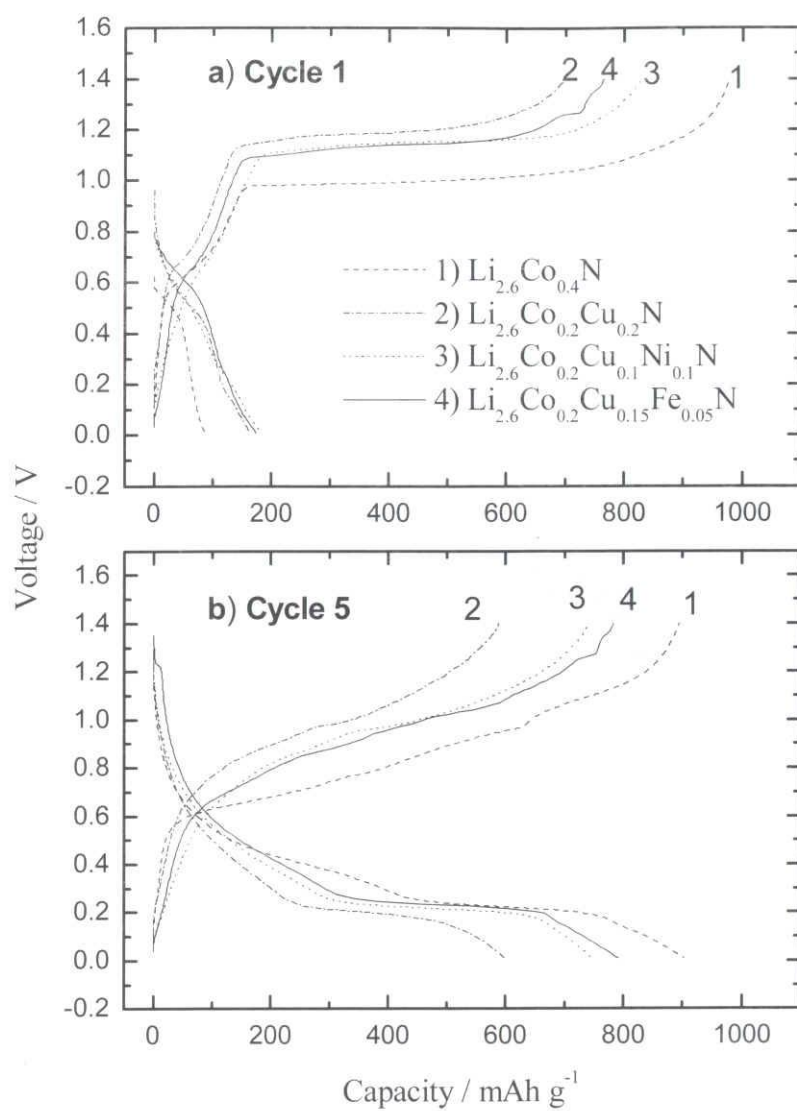
Fig.21. Charge and discharge profiles of the lithium metal nitrides electrodes at a) cycle 1 and b) cycle 5.
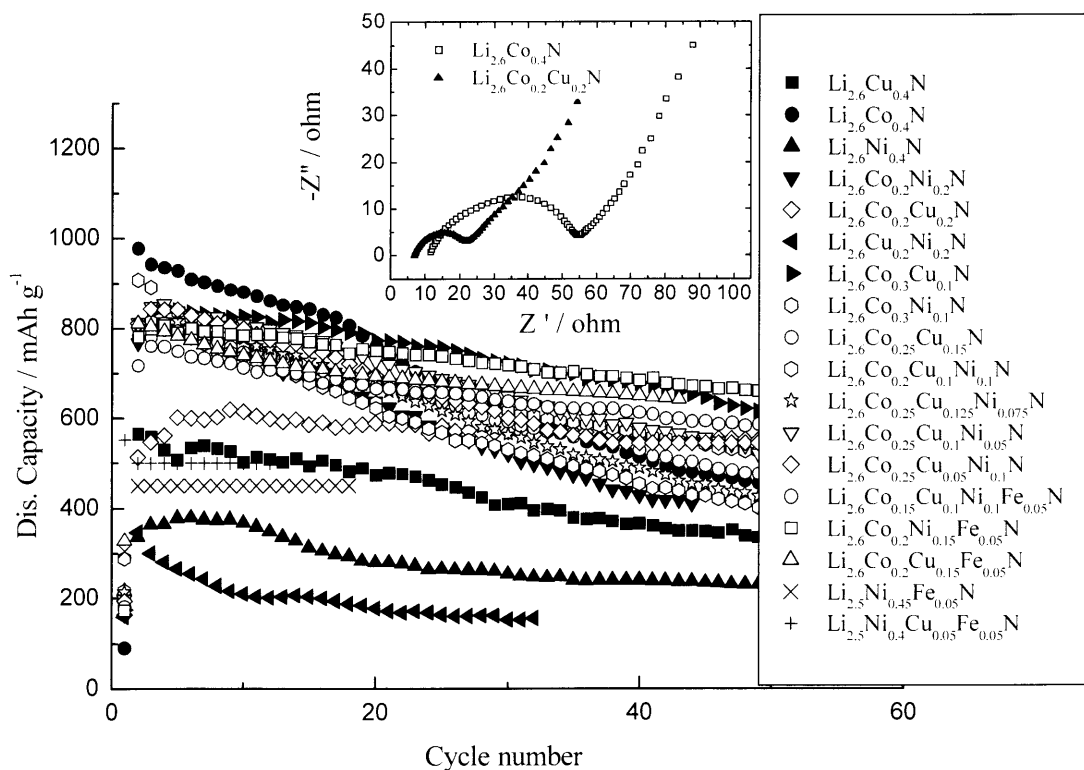
Fig.22 Cycling performance of the lithium metal nitrides electrodes. The inset figure is Cole-Cole plots of the impedance response of the a) $Li_{2.6}Co_{0.4}N$ and b) $Li_{2.6}Co_{0.2}Cu_{0.2}N$ with the charged state after 30 cycles.
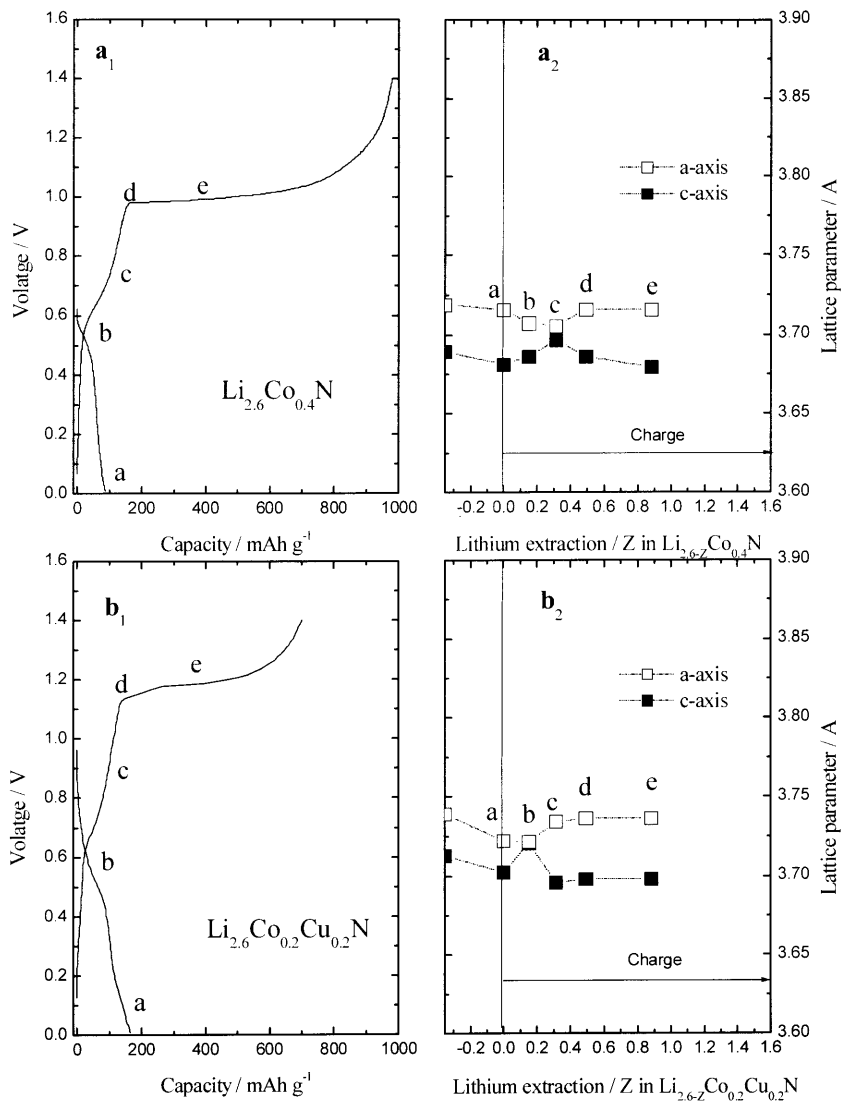
Fig.23. Variation of lattice parameters of the a) $Li_{2.6}Co_{0.4}N$ and b) $Li_{2.6}Co_{0.2}Cu_{0.2}N$ with various Li-insertion/extraction depths in the first cycle.
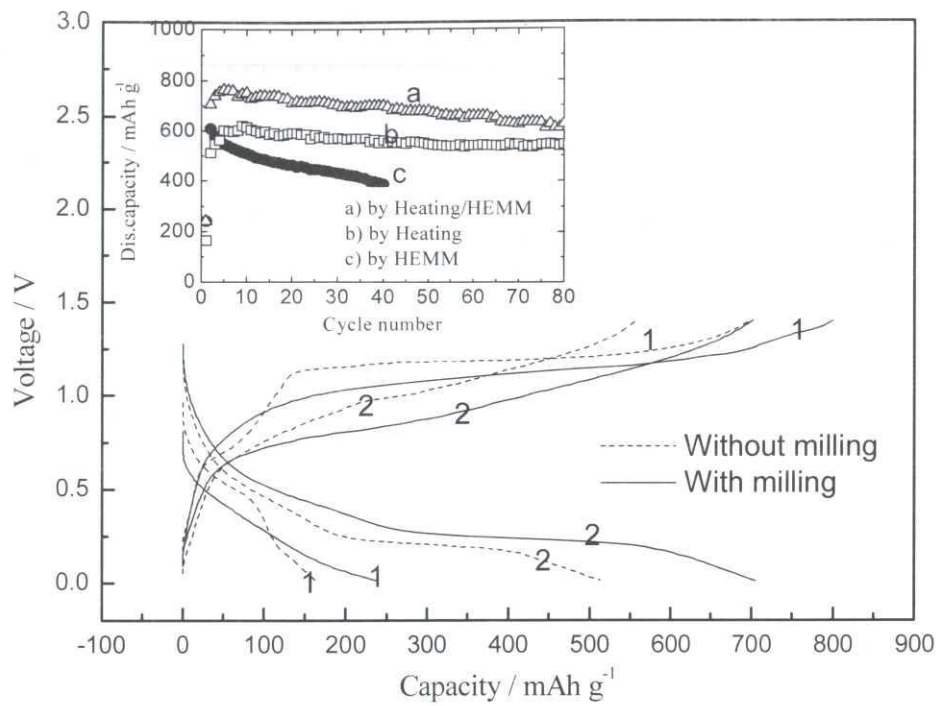
Fig.24. Charge and discharge curves of the electrodes based on $Li_{2.6}Co_{0.2}Cu_{0.2}N$ without and with HEMM at the first and the second cycle. The inset figure is Cycling performance of the electrodes of the $Li_{2.6}Co_{0.2}Cu_{0.2}N$ under different preparations.
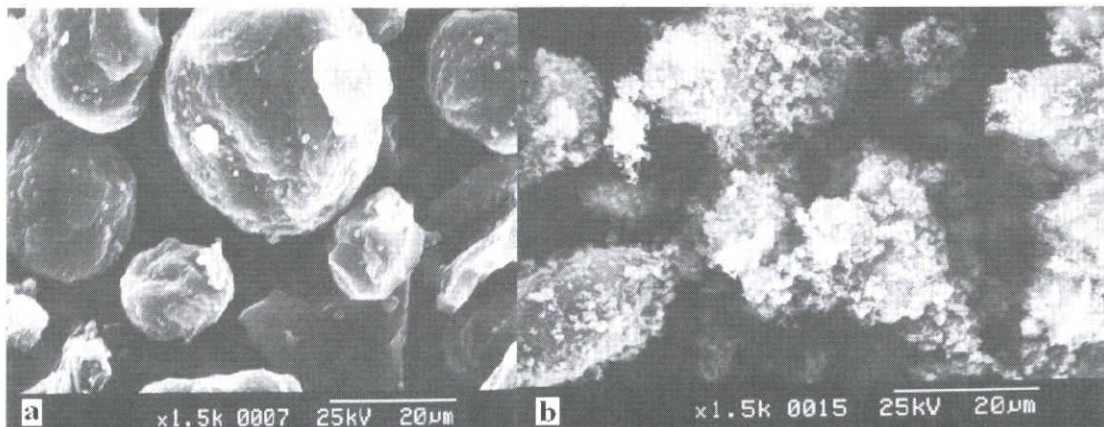
Fig.25. SEM photos of a) the mechanical mixture of MCMB-$Li_{2.6}Co_{0.4}N$ and b) the HEMM MCMB-$Li_{2.6}Co_{0.4}N$ composite prepared by HEMM.
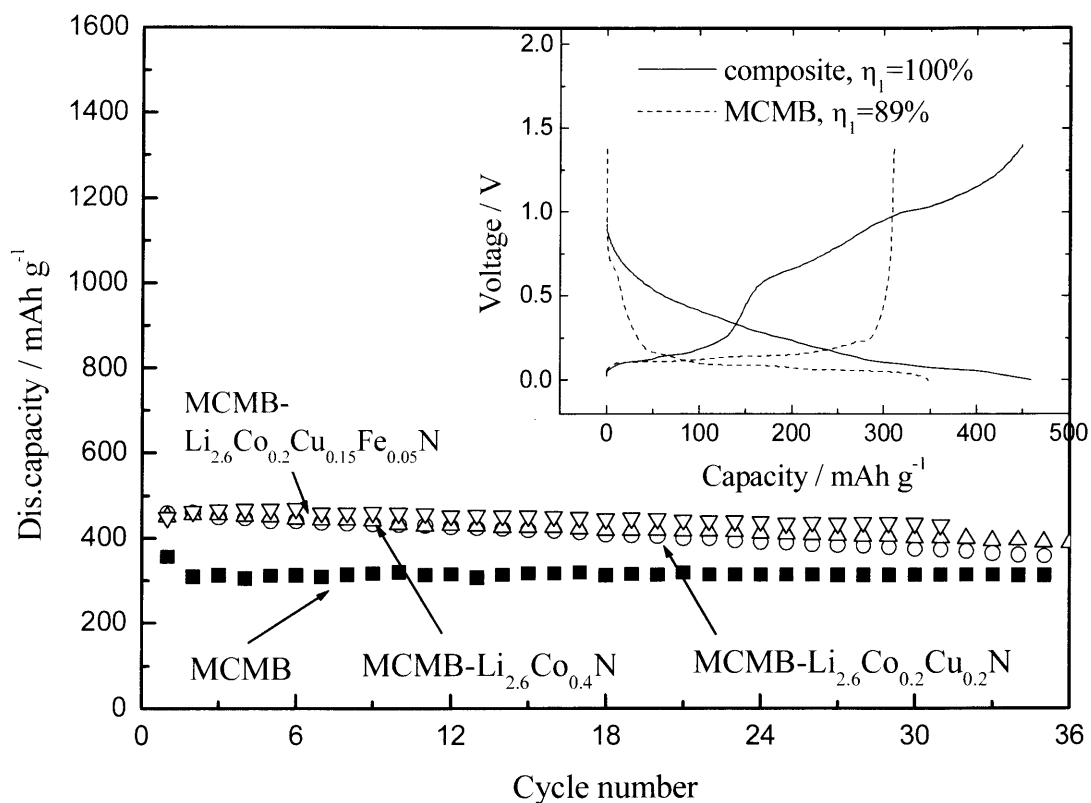
Fig.26. Cycling performance of the lithium metal nitrides-MCMB composites and the MCMB electrodes. The inset figure is charge and discharge curves of the $Li_{2.6}Co_{0.4}N$-MCMB composite and the MCMB electrodes at the first cycle.
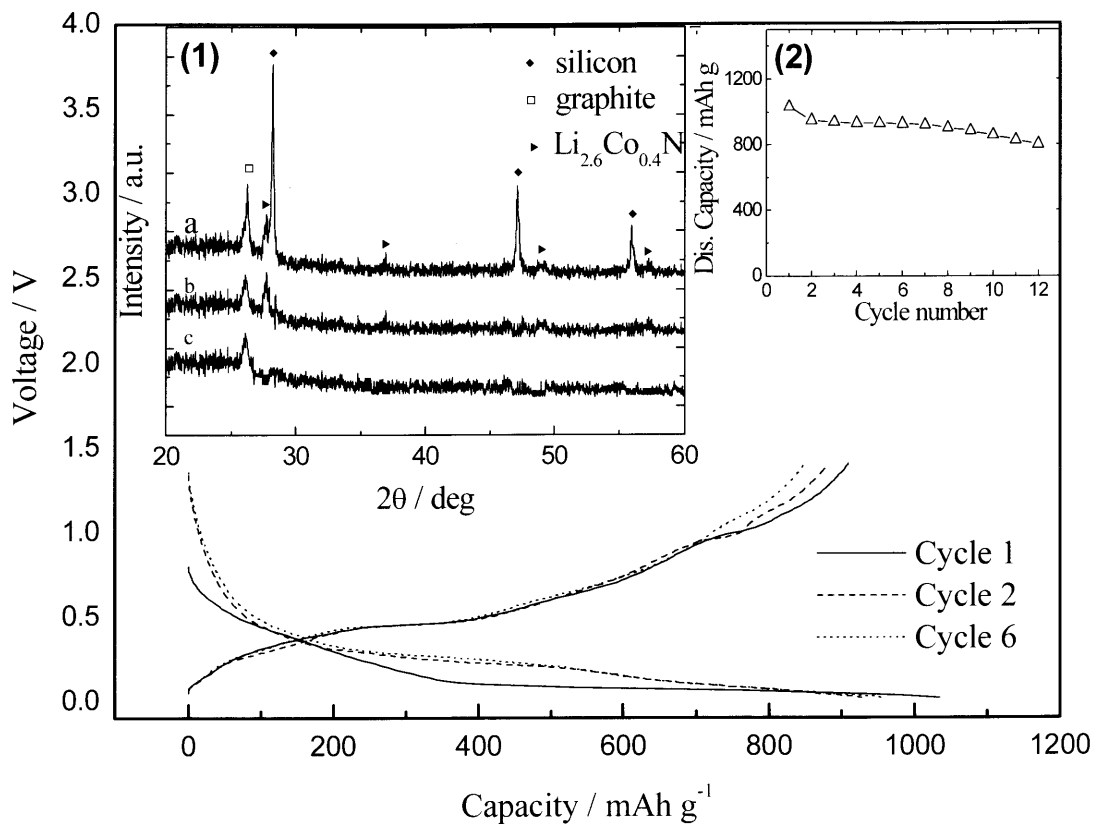
Fig.27. Charge and discharge curves of the Si–graphite–$Li_{2.6}Co_{0.4}N$ composite electrode at different cycles. The inset figure (1) is XRD patterns of the Si–graphite–$Li_{2.6}Co_{0.4}N$ composite electrode: (a) before charge and discharge, (b) after first discharge and (c) after first discharge. The inset figure (2) is cycling performance of the Si–C–$Li_{2.6}Co_{0.4}N$ composite.
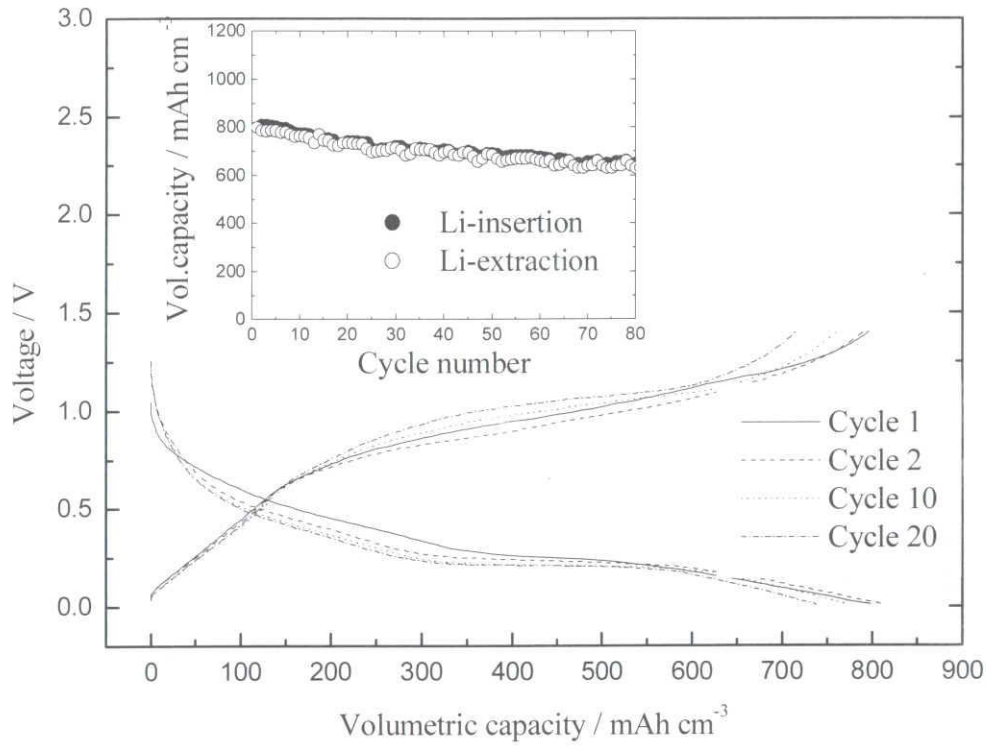
Fig.28. Charge and discharge profiles of the $Li_{2.6}Co_{0.4}N$-$LiTi_2O_4$ electrode at different cycles. The inset figure is the cycling performance.
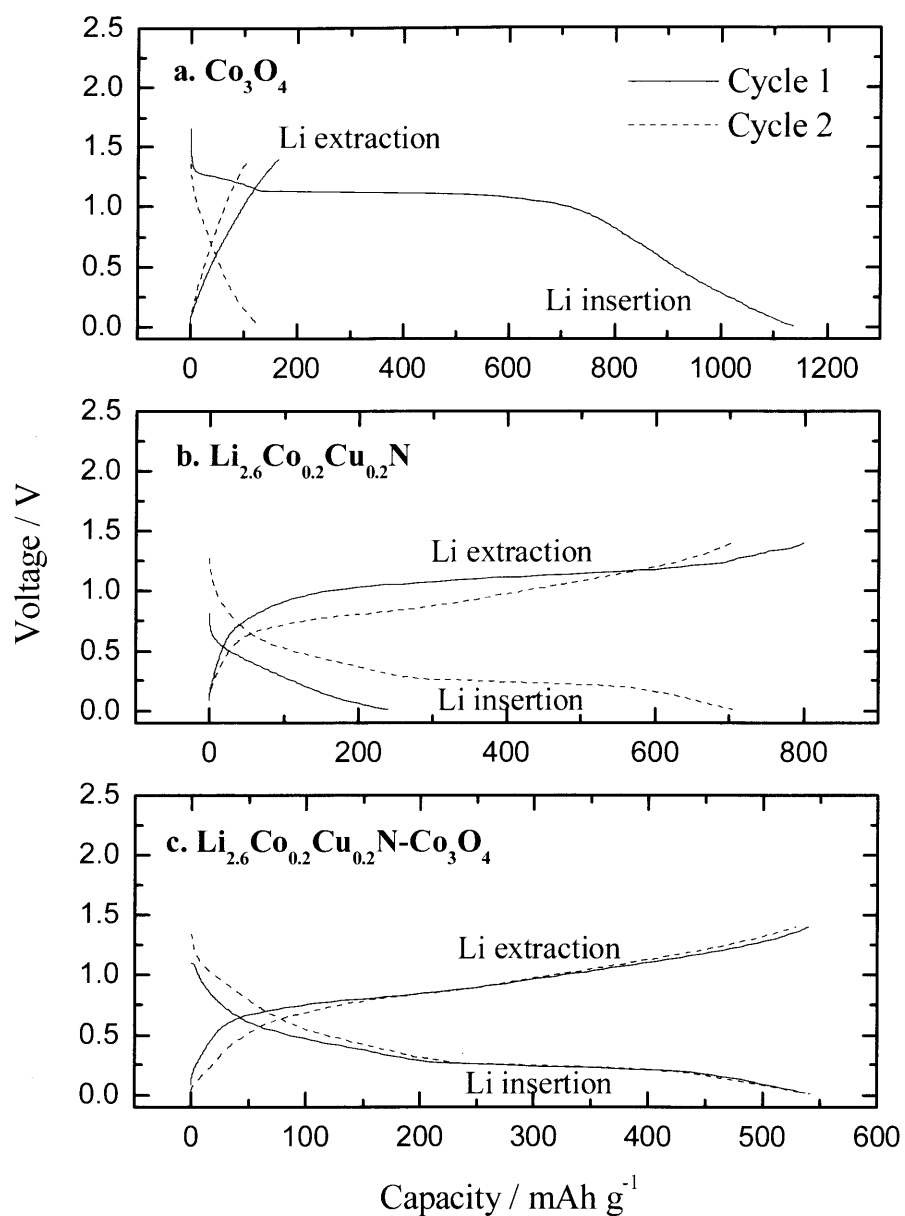
Fig.29. Charge-discharge curves of the cells: a) Co_3O_4 / electrolyte / Li, b) $Li_{2.6}Co_{0.2}Cu_{0.2}N$ / Electrolyte / Li and c) Co_3O_4 - $Li_{2.6}Co_{0.2}Cu_{0.2}N$ (37.5 - 62.5 wt. %) / electrolyte/ Li at room temperature.
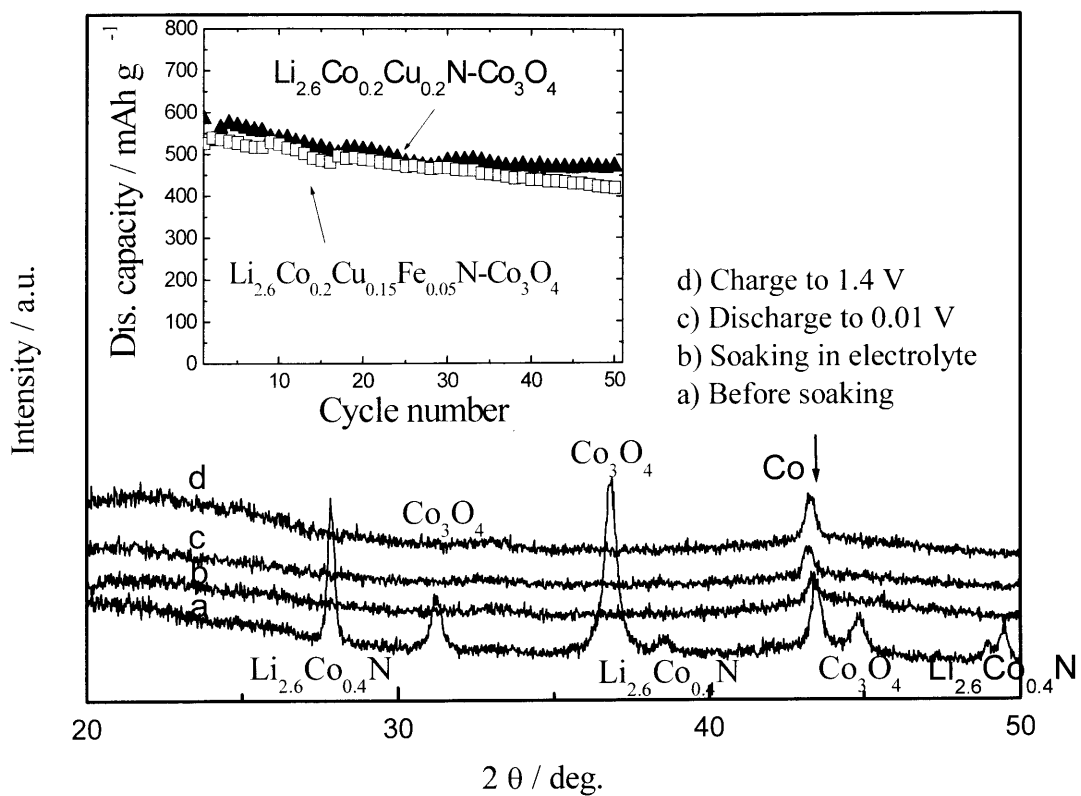
Fig.30. XRD patterns of the Co_3O_4-$Li_{2.6}Co_{0.2}Cu_{0.2}N$ composite electrode at different stages. The inset figure is cycling performance of the composites.
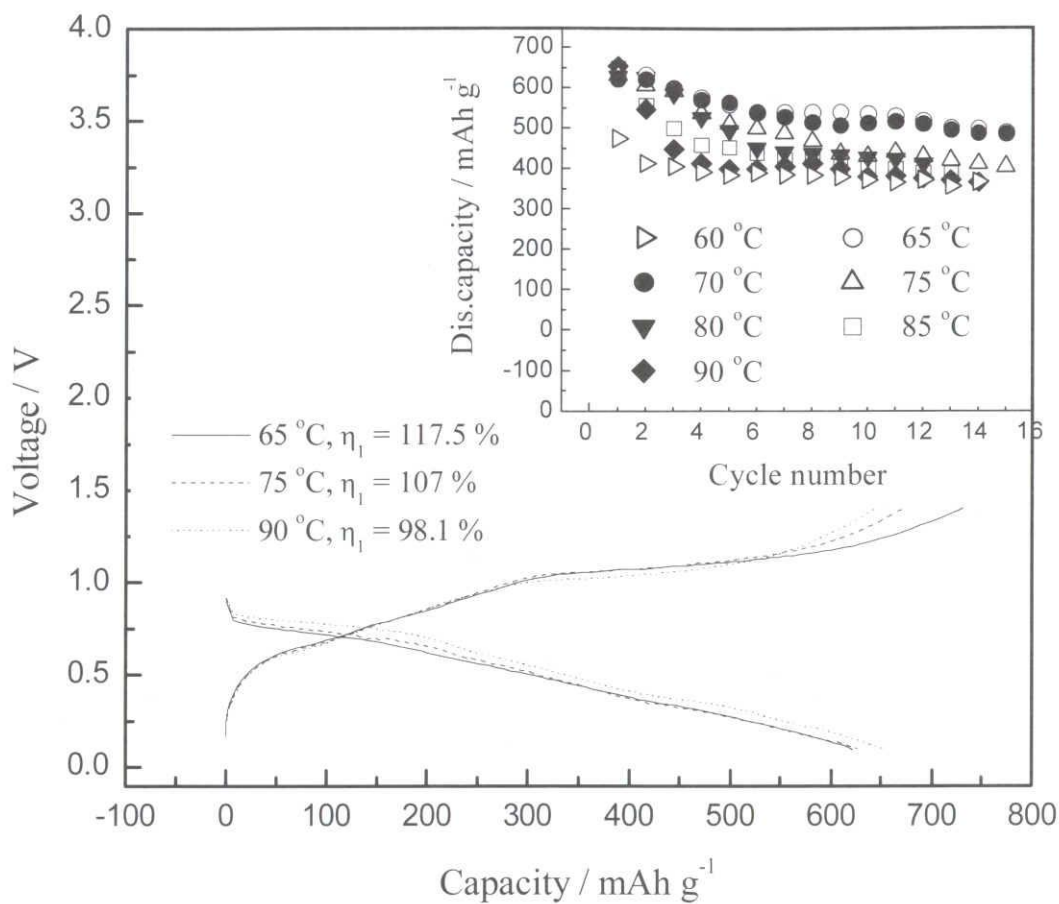
Fig.31. The first charge and discharge profiles of composite electrodes at different operating temperature. The inset figure is cycling performance of composite electrodes at different operating temperature.
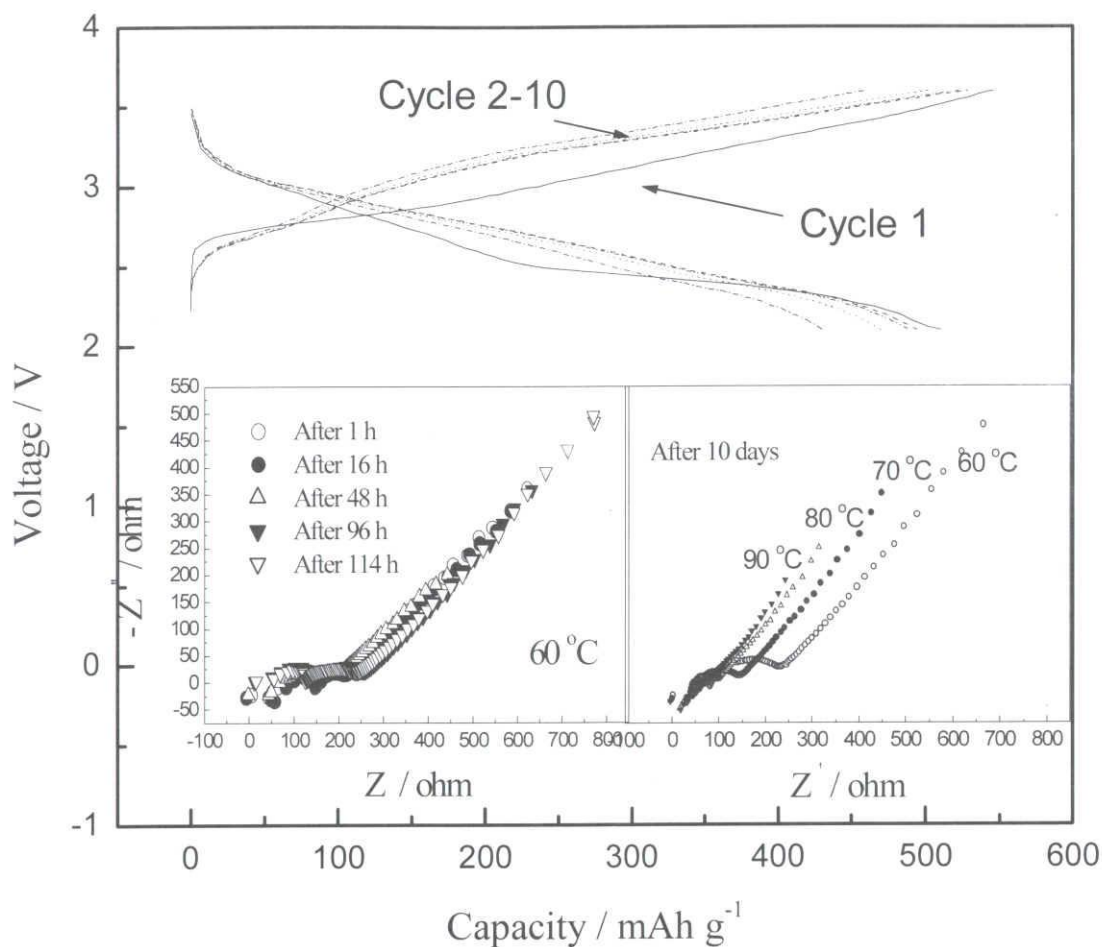
Fig.32. Charge and discharge profiles of coin type cell using LiNi$_{0.8}$Co$_{0.2}$O$_2$ cathode and composite anode in solid electrolytes at 65℃. Voltage cut off: 2.1-3.6 V, i$_c$=i$_d$=0.1 mA cm^{-2}. The inset figure (1) is impedance performances of composite electrodes storage at 60℃ at different time. The inset figure (2) is impedance performances of composite electrodes during storage at different operating temperature.
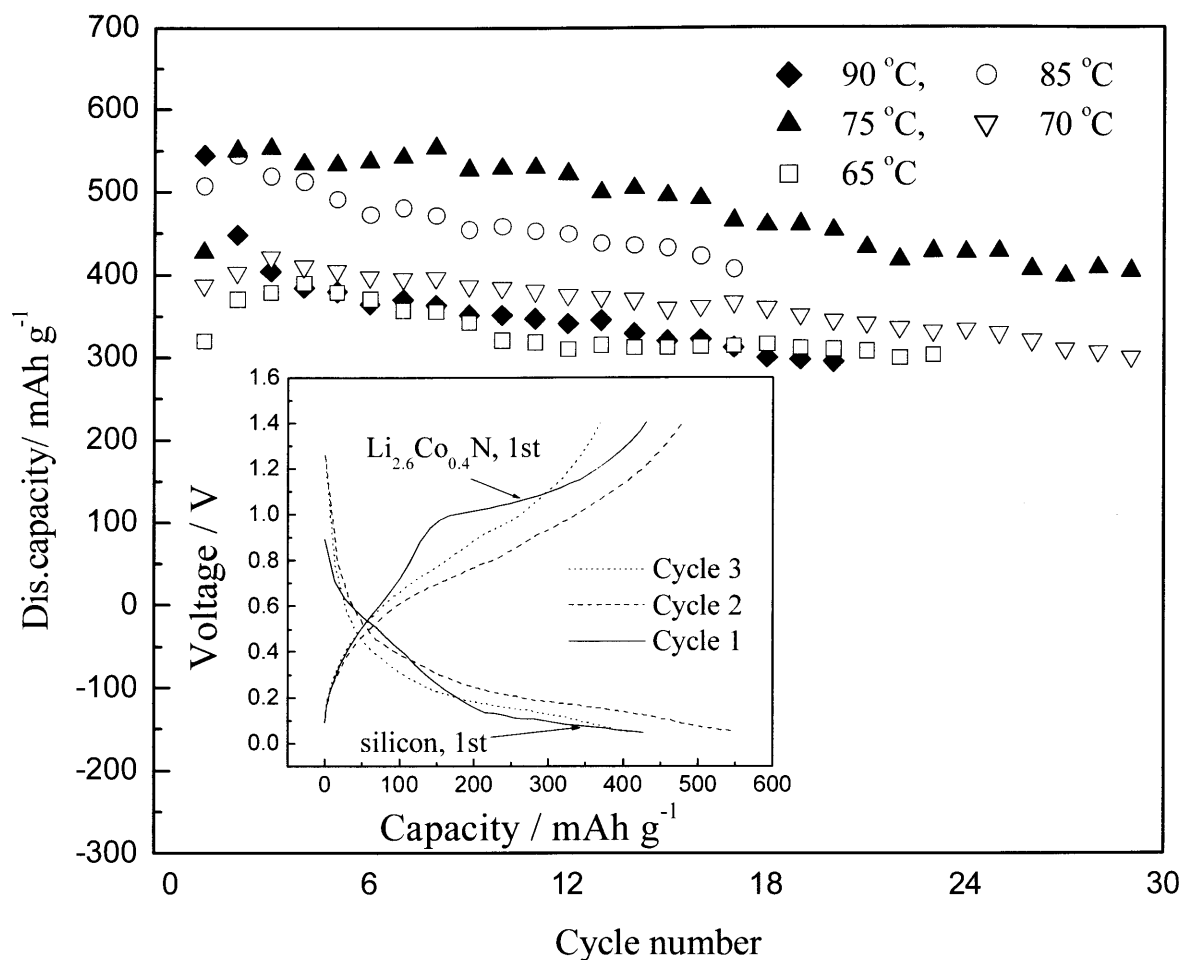
Fig.33. Cycling performance of the composite electrodes at different temperature. The inset figure is charge and discharge curves of the $SiO_{1.1}$-$Li_{2.6}Co_{0.4}N$ composite electrode at different cycles.

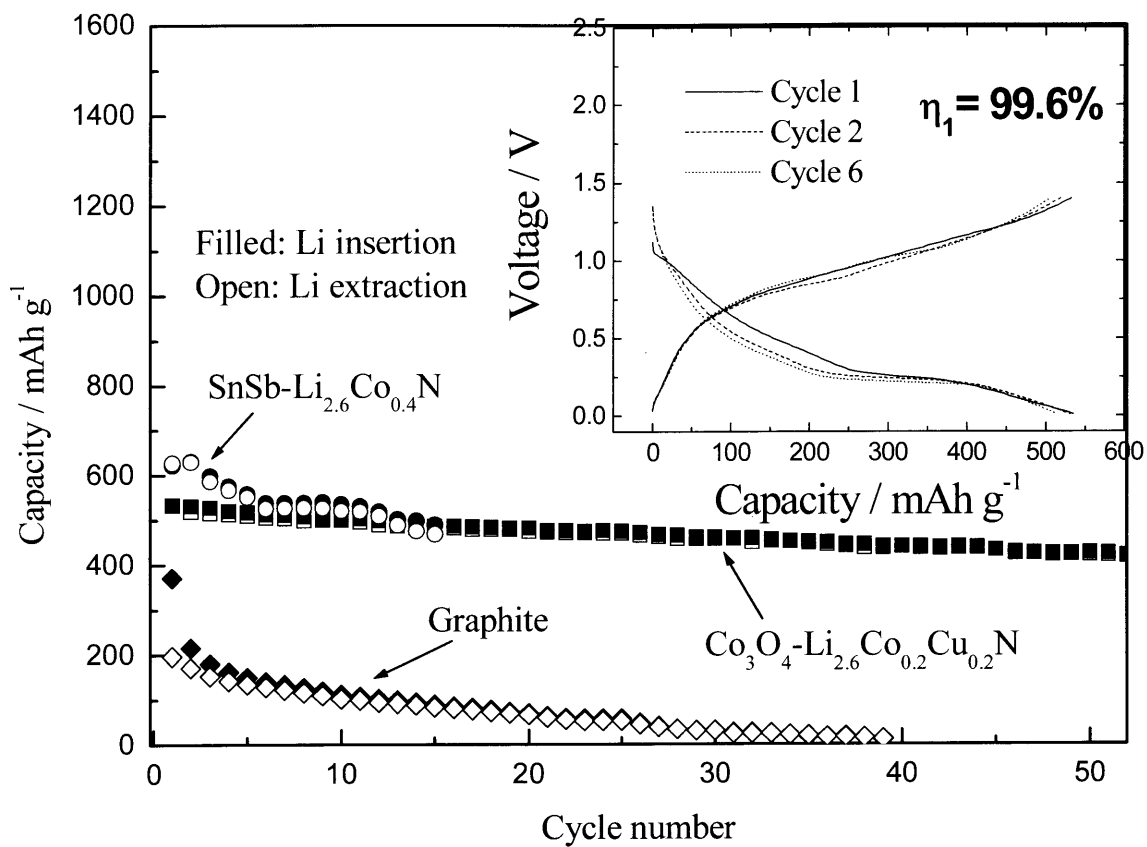Fig.34. Cycling performance of SnSb-Li$_{2.6}$Co$_{0.4}$N, Co$_3$O$_4$-Li$_{2.6}$Co$_{0.2}$Cu$_{0.2}$N and graphite with PEO electrolytes vs. Li at 65 ℃. The inset figure is charge and discharge profiles of the Co$_3$O$_4$-Li$_{2.6}$Co$_{0.2}$Cu$_{0.2}$N electrode.

参考：
当研究室で発表したリチウム二次電池用新規負極材料(コンポジット正極も含む)関係の論文、学会発表のリスト。

1. K.Hanai,Y.Liu,T.matsumura,N.Imanishi,A.Hirano,Y.Takeda, "Electrochemical behavior of the composite anodes consisting of carbonaceous materials and lithium transition-metal nitrides for lithium-ion batteries" Solid State Ionics, 2008 in press

2. N. Imanishi, Y. Ono, K. Hanai, R. Uchiyama, Y. Liu, A. Hirano, Y. Takeda, O. Yamamoto, "Surface-modified meso-carbon microbeads anode for dry polymer lithium-ion batteries" Journal of Power Sources, 178, 744-750 (2008)

3. J. Xie, N. Imanishi, A. Hirano, M. Matsumura, Y. Takeda, O. Yamamoto,"Orientation dependence of Li-ion diffusion kinetics in $LiCoO_2$ thin films prepared by RF magnetron sputtering" Solid State Ionics, 179, 362-370(2008)

4. J. Xie, N. Imanishi, A. Hirano, M. Matsumura, Y. Takeda, O. Yamamoto, "Kinetics investigation of a preferential (104) plane oriented $LiCoO_2$ thin film prepared by RF magnetron sputtering" Solid State Ionics, 178, 1218-1224(2007)

5. T.Matsumura,K.Nakano,R.Kanno,A.Hirano,N.Imanishi,Y.takeda, "Nickel sulfides as a cathode for all-solid-state ceramic lithium batteries" J. Power Sources, 174, 632-636(2007)

6. Y.Liu, Y.Takeda, T.Matsumura, J.Yang, N.Imanishi, O.Yamamoto, "Novel composite anodes consisting of lithium transition-metal nitrides and transition metal oxides for rechargeable Li-ion batteries." J.Electrochem.Soc., 153, A437-A444 (2006)

7. N.Imanishi, K.Shizuka, T.Ikenishi, T.Matsumura, A.Hirano, Y.Takeda, "Preparation and electorochemical properties of a Li_2CuO_2-Li_2NiO_2 solid solution as a lithium intercalation electrode" Solid State Ionics, 177, 1341-1346(2006)

8. Y. Liu, J. Yang, N. Imanishi, A. Hirano, Y. Takeda and O. Yamamoto, "Composite anode containing nano-$SiO_{1.1}$ and $Li_{2.6}Co_{0.4}N$ with solid PEO electrolytes for lithium-ion batteries", J. Power Sources, 146 (2005), 376

9. Y. Liu, T. Matsumura, N. Imanishi, A. Hirano, T. Ichikawa and Y. Takeda, "Preparation and characterization of Si/C composite coated with polyaniline as novel anodes for Li-ion batteries", Electrochemical and Solid-State Letters, 8 (11) 2005.

10. K. Hanai, Y. Liu, N. Imanishi, T. Ichikawa, A. Hirano and Y. Takeda, "Electrochemical studies of the Si-based composites with large capacity and good cycling stability as anode materials for rechargeable lithium ion batteries", J. Power Sources, 146 (2005), 156

11. Y. Liu, K. Horikawa, M.Fujiyosi, N. Imanishi, A. Hirano and Y. Takeda, "The study of doped elementals upon the electrochemical behaviors of the hexagonal $Li_{2.6}Co_{0.4}N$", J. Electrochem. Soc., 151 (2004) A1450.

12. Y. Liu, K. Hanai, T. Matsumura, N. Imanishi, A. Hirano and Y. Takeda, "Novel composites based

on ultrafine silicon, carbonaceous matrix and the introduced co-milling components as anode host materials for lithium ion batteries", Electrochemical and Solid-State Letters, 7 (2004) A492.

13. Y. Liu, T. Matsumura, N. Imanishi, T. Ichikawa, A. Hirano, Y. Takeda, "Lithium transition metal nitrides with the modified morphology characteristics as advanced materials for lithium ion batteries", Electrochemistry Communications 6 (2004) 632.

14. Y. Liu, K. Horikawa, M. Fujiyoshi, T. Matsumura, N. Imanishi and Y. Takeda, "Novel composite anodes based on layered lithium transition metal nitrides for lithium secondary batteries", Solid State Ionics, 172 (2004) 69.

15. Y. Liu, K. Horikawa, M. Fujiyosi, N. Imanishi, A. Hirano and Y. Takeda, "Layered lithium transition metal nitrides as novel anodes for lithium secondary batteries", Electrochimica Acta 49 (2004) 3487.

16. Y. Liu, K. Hanai, J. Yang, N. Imanishi, A. Hirano and Y. Takeda, "Novel silicon/carbon composites as anode materials for Li-ion batteries", Electrochemical and Solid-State Letters, 7, (2004) A369.

17. Y. Liu, K. Hanai, K. Horikawa, N. Imanishi, A. Hirano and Y. Takeda, "Electrochemical characterization of a novel Si-graphite-$Li_{2.6}Co_{0.4}N$ composite as anode material for lithium secondary batteries", Materials Chemistry & Physics, 89 (2004) 80.

18. Y. Liu, J. Yang, N. Imanishi, A. Hirano, Y. Takeda, and O. Yamamoto, "Novel Solid-State Cells $LiNi_{0.8}Co_{0.2}O/PEO/SnSb-Li_{2.6}Co_{0.4}N$ Without Metallic Lithium", J. Ceramic Society of Japan, 112 (2004) s638.

19. Y. Liu, K. Hanai, J. Yang, N. Imanishi, A. Hirano, Y. Takeda, "Morphology-stable silicon based composite for Li-intercalation", Solid State Ionics, 168 (2004) 61-68.